THE ASTRONOMICAL JOURNAL, 124:2721–2738, 2002 November

E

THE PALOMAR/MSU NEARBY STAR SPECTROSCOPIC SURVEY. IV. THE LUMINOSITY FUNCTION IN THE SOLAR NEIGHBORHOOD AND M DWARF KINEMATICS[1]

I. NEILL REID
Space Telescope Science Institute, 3700 San Martin Drive, Baltimore, MD 21218; and Department of Physics and Astronomy, University of Pennsylvania, 209 South 33d Street, Philadelphia, PA 19104-6396; inr@stsci.edu

JOHN E. GIZIS
Department of Physics and Astronomy, University of Delaware, Newark, DE 19716; gizis@udel.edu

AND

SUZANNE L. HAWLEY
Department of Astronomy, University of Washington, Box 351580, Seattle, WA 98195; slh@pillan.astro.washington.edu
Received 2002 July 1; accepted 2002 July 25

ABSTRACT

We have used new astrometric and spectroscopic observations to refine the volume-complete sample of M dwarfs defined in previous papers in this series. With the addition of *Hipparcos* astrometry, our revised VC^2 sample includes 558 main-sequence stars in 448 systems. Analysis of that data set shows no evidence of any systematic kinematic bias. Combining those data with a *Hipparcos*-based sample of AFGK dwarfs within 25 pc of the Sun, we have derived the solar neighborhood luminosity function, $\Phi(M_V)$, for stars with absolute magnitudes between -1 and $+17$. Using empirical and semiempirical mass-M_V relations, we transform $\Phi(M_V)$ to the present-day mass function, $\psi(M)$ $(=dN/dM)$. Depending on the mass-luminosity calibration adopted, $\psi(M)$ can be represented by either a two-component or a three-component power law. In either case, the power-law index α has a value of $\sim$1.3 at low masses ($0.1\ M_\odot < M < 0.7\ M_\odot$), and the local mass density of main-sequence stars is $\sim$0.031 $M_\odot$ pc^{-3}. We have converted $\psi(M)$ to an estimate of the initial mass function, $\Psi(M)$, by allowing for stellar evolution, the density law perpendicular to the plane, and the local mix of stellar populations. The results give $\alpha = 1.1$–1.3 at low masses and $\alpha = 2.5$–2.8 at high masses, with the change in slope lying between 0.7 and 1.1 $M_\odot$. Finally, the (U, W) velocity distributions of both the VC^2 sample and the fainter ($M_V > 4$) stars in the *Hipparcos* 25 pc sample are well represented by two-component Gaussian distributions, with $\sim$10% of the stars in the higher velocity dispersion component. We suggest that the latter component is the thick disk, and we offer a possible explanation for the relatively low velocity dispersions shown by ultracool dwarfs.

Key words: solar neighborhood — stars: kinematics — stars: luminosity function, mass function
On-line material: color figures, machine-readable tale

1. INTRODUCTION

The nearest stars represent an important tool in studies of Galactic structure, since they provide an opportunity for detailed analysis of constituent members of the various stellar populations and subpopulations. This holds particularly for M dwarfs, which account for the overwhelming majority of stars currently present in the Galaxy. With a local density of $\sim$0.07 pc^{-3}, these stars are ideal tracers of many properties of the Galactic disk. Until recently, the main limitation in such analyses was the lack of basic observational data, such as spectral types or radial velocities. Our main goal in undertaking the Palomar/Michigan State University (PMSU) survey (Reid, Hawley, & Gizis 1995, hereafter PMSU1; Hawley, Gizis, & Reid 1996, hereafter PMSU2; Hawley, Gizis, & Reid 1997) was to remedy this defect by compiling moderate-resolution spectroscopy for all M dwarfs in the preliminary version of the Third Catalogue of Nearby Stars (pCNS3; Gliese & Jahreiss 1991). We obtained observations of over 2000 candidate M dwarfs, omitting only unresolved binary companions. Calculating distances by combining spectroscopic parallaxes with the then available trigonometric data, we defined M_V-dependent distance limits that isolate a volume-complete sample and used that sample to derive estimates of the luminosity function and the velocity distribution of low-mass stars (PMSU1), in addition to studying the range of chromospheric activity (PMSU2).

Since the completion of our initial analysis, two major new data sets have become available. First, the *Hipparcos* Catalogue has been published (ESA 1997), including milliarcsecond-accuracy astrometry for over 110,000 stars brighter than 13th magnitude. Almost two-thirds of the stars in the pCNS3 have observations by *Hipparcos*. Second, as a follow-up to the PMSU survey, we obtained echelle spectroscopy of many of the brighter M dwarfs in the pCNS3, including all of the stars in the volume-complete sample defined in PMSU1. Those data are now fully analyzed and are presented in Gizis, Reid, & Hawley (2002, hereafter PMSU3). The high-resolution observations provide significantly more accurate radial velocities, besides more sensitive measurement of chromospheric activity.

Both these new data sets have potential importance for the results of the analysis presented in PMSU1. Revising the

[1] Based partly on observations made at the 60 inch (1.5 m) telescope at Palomar Mountain, which is jointly owned by the California Institute of Technology and the Carnegie Institution of Washington.

distances of a substantial number of stars affects both the composition of the volume-complete sample and the derived tangential motions, while the new radial velocity determinations affect the space motion determinations. We have therefore reanalyzed the PMSU data set, incorporating the new observational data. Section 2 describes the definition of the revised volume-complete sample; § 3 considers the effect on the luminosity function; § 4 rederives the mass function for nearby stars, combining our data with a *Hipparcos* 25 pc sample of earlier-type main-sequence stars; and § 5 reanalyzes the kinematics. The main results are summarized and discussed in § 6.

2. A VOLUME-COMPLETE SAMPLE OF SOLAR NEIGHBORHOOD M DWARFS

In PMSU1, we used the available trigonometric and photometric parallax information, together with our own distance estimates based on the (M_V, TiO5) calibration, to construct a volume-complete (VC) subset of the M dwarfs in the pCNS3. Over 2300 pCNS3 stars have *Hipparcos* astrometry, but with incomplete sampling between $V = 8$ and the *Hipparcos* limit of $V = 13$ that data set includes only 712 M dwarfs from PMSU1 and PMSU2. Coverage is better among the brighter stars in the PMSU1 VC subset, however, with data for 330 of the 499 systems.

Figure 1 compares pre- and post-*Hipparcos* distance measurements for PMSU stars; there is a systematic shift toward higher distances (parallaxes tend to be overestimated, hence the Lutz-Kelker bias), and a significant number of M dwarfs move beyond the 25 pc boundary of the pCNS3. Seventy-one of the 499 systems in the VC sample have revised distances that place the stars beyond the completeness limits adopted for the appropriate absolute magnitude. We have therefore reanalyzed the pCNS3 data set, augmented by new observations, and derive a revised volume-complete sample of M dwarfs (VC^2).

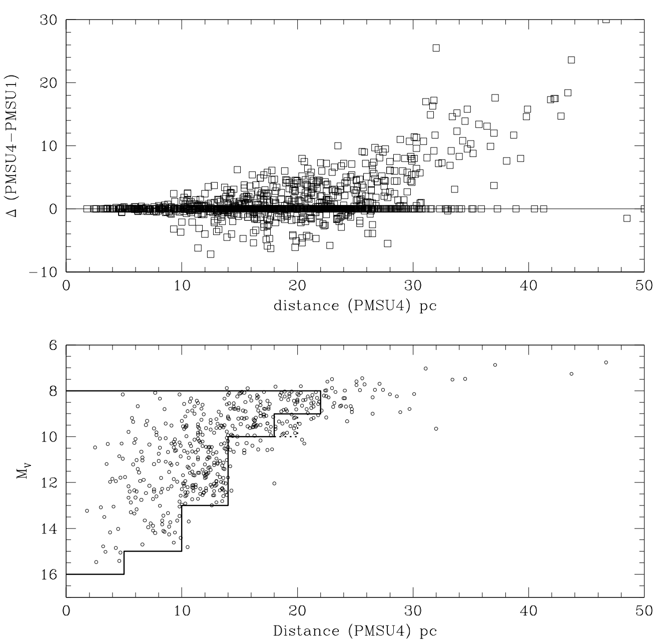

FIG. 1.—Comparison between distance determinations pre- and post-*Hipparcos*. The top panel plots the difference, $\Delta d = d_{\rm PMSU4} - d_{\rm PMSU1}$, for the 1684 M dwarfs. The bottom panel shows the effect on the original VC sample, plotting the revised distances and absolute magnitudes in comparison with the PMSU1 distance limits. Seventy-one of 499 systems fall outwith the formal sampling volume.

2.1. *Redefining the Sample*

We have used the techniques described in PMSU1 to analyze the post-*Hipparcos* pCNS3 data set, rederiving the appropriate distance limits as a function of absolute magnitude. As before, we limit analysis to the 1684 M dwarf systems in the northern sample, $\delta > -30°$, and set absolute magnitude limits $8 < M_V \leq 16$. Figure 2 provides the justification for our choice of distance limits, plotting the run of density ($\rho_{\rm sys}$, number of *systems* per unit volume) with increasing distance; the distance limits, $d_{\rm lim}$, are set where $\rho_{\rm sys}$ flattens, before the downturn due to incompleteness. Applying Schmidt's (1968) $V/V_{\rm max}$ estimator to the same issue yields identical results.

As Table 1 shows, the revised distance limits match those derived in PMSU1, with the exception of the $M_V = 9.5$ bin, where $d_{\rm lim}$ decreases by 10%. A total of 545 stars in 435 systems, including 300 with *Hipparcos* data, meet these distance criteria. This data set includes additional companions identified by Reid & Gizis (1997, hereafter RG97), Delfosse et al. (1999), and Beuzit et al. (2001). Only 16 systems lack PMSU3 echelle observations, and the majority (381 systems) have distances derived from trigonometric parallaxes. The relevant data for each stellar system are listed in Table 2, where we also give the proper motions and space velocities.

Besides providing improved distance estimates for stars already known to lie within the immediate solar neighborhood, *Hipparcos* also identified a number of previously unrecognized nearby stars. The full catalog lists 78 stars that are not in the pCNS3 but have $\pi_{\rm H} > 45$ mas, or $r < 22$ pc. Of these, 23 have formal absolute magnitude values in the range $8 < M_V \leq 16$. Ten of the latter subset, however, have spectral types that are clearly inconsistent with the inferred absolute magnitude; for example, HIP 21000, or BD +4°701A, has $\pi_{\rm H} = 84.8$ mas and an inferred $M_V = 9.5$, but spectral type F8. All 10 are in binary systems, and the companion has influenced the astrometric results listed in the *Hipparcos* Catalogue. This is a well-known problem, which can be rectified through more sophisticated analysis; thus, Fabricius & Makarov (2000) derive $\pi'_H = 4.2$ mas for HIP 21000.

The remaining 13 stars in the supplementary sample are all confirmed M dwarfs. The parallax measurements for both Vyssotsky 130 (a double star) and HD 218422 have substantial uncertainties. For the present, we retain both stars in the sample, increasing the revised VC^2 sample to 558 main-sequence stars[2] in 448 systems. Relevant data for the additional stars are listed in Table 3. With the exception of LHS 1234 (Weis 1996) prior observations are scarce, and most lack radial velocity data. For those stars, the space motions listed in Table 3 are computed for $V_r = 0$ km s^{-1}.

2.2. *Biases and Completeness*

A reliable determination of the properties of the local Galactic disk demands an unbiased, representative stellar

[2] There are an additional four white dwarf and three brown dwarf companions.

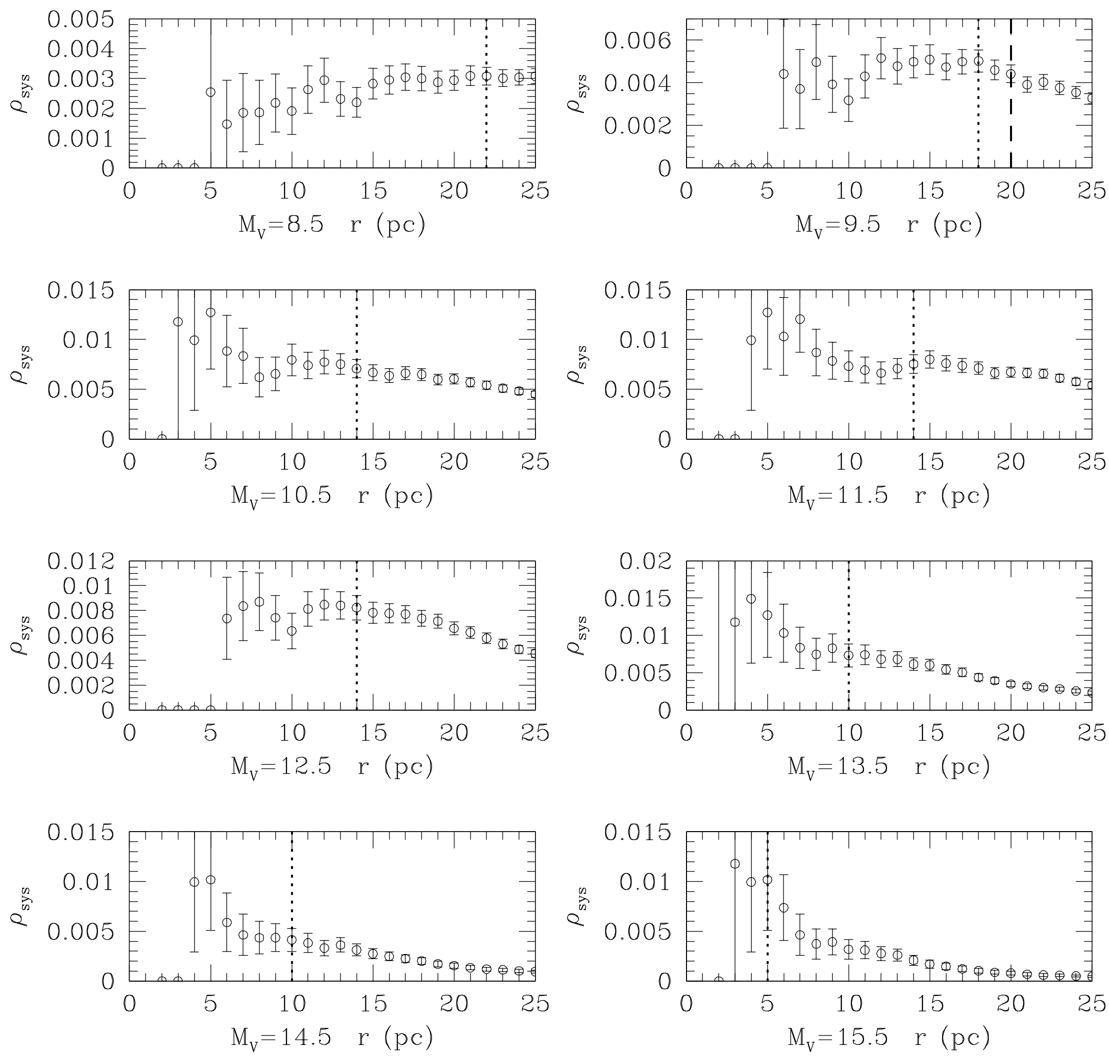

FIG. 2.—Run of density with increasing distance for pCNS3 M dwarfs as a function of absolute magnitude. The dotted vertical lines mark the distance limits for the volume-complete sample; the dashed vertical line for $M_V = 9.5$ marks the value adopted in Paper I.

data set. It is to that end that we constructed the VC^2 sample described in the previous section. However, while the $\rho(d)$ and $(V/V_{\max})(d)$ measurements show that the sample as a whole is broadly consistent with our requirements, subtle biases may remain, particularly since the stars are drawn primarily from a preexisting catalog (the pCNS3) rather than an unbiased all-sky survey. On the positive side, our VC^2 sample has the advantage that trigonometric parallax measurements are the dominant contributor to distance estimates for 90% of the systems. This is in contrast to the original PMSU1 VC sample, where 40% of the stars lacked accurate astrometry.

TABLE 1
DISTANCE LIMITS

M_V	$d_{\rm orig}$ (pc)	$d_{\rm lim}$ (pc)
8.5	22	22
9.5	20	18
10.5	14	14
11.5	14	14
12.5	14	14
13.5	10	10
14.5	10	10
15.5	5	5

NOTE.—Here $d_{\rm orig}$ lists the distance limit adopted in PMSU1, and $d_{\rm lim}$ is the distance limit adopted in the present analysis.

Two potential sources of bias are proximity to the Galactic plane, where crowding might be a problem leading to omission of nearby stars, and proper-motion–based selection, which could bias against nearby stars with low space motions. Considering the former issue, Figure 3 plots the distribution of the VC^2 sample on the celestial sphere. Based on the areal coverage, we expect 15.9% of the sample to lie within $\pm 10^\circ$ of the Galactic plane; in fact, 69 of the 448 systems (15.4% $\pm$ 1.9%) lie within those limits. We conclude that crowding in the Galactic plane is not a significant contributor to incompleteness in the VC^2 sample.[3]

[3] We note that there *is* a statistically significant bias against low-latitude systems if we consider low-luminosity stars in the full pCNS3: of the 395 stars north of -30° with $M_V > 13$, only 41, or 10.4% $\pm$ 1.8%, lie within 10° of the plane. The distance and M_V limits imposed in defining the VC^2 sample have eliminated this potential source of bias.

TABLE 2

BASIC DATA FOR THE VC SAMPLE

No. (1)	Name (2)	Distance (pc) (3)	Ref. (4)	M_V (5)	V_r (km s^{-1}) (6)	μ_α (arcsec yr^{-1}) (7)	μ_δ (arcsec yr^{-1}) (8)	U (km s^{-1}) (9)	V (km s^{-1}) (10)	W (km s^{-1}) (11)	Hα (Å) (12)	Comments (13)
7.......	Gl 2	11.5 ± 0.1	1	9.63	0.4	0.879	−0.163	−39.4	−23.3	−16.6	−0.40	
11.....	Gl 4A	11.8 ± 0.4	1	8.61	3.3	0.821	−0.172	−38.7	−20.0	−17.7	−0.57	
19.....	GJ 1002	4.6 ± 0.0	2	15.42	−40.1	−0.817	−1.870	36.7	−39.5	26.1	0.11	94/6
41.....	GJ 1005A	5.6 ± 0.2	1	12.84	−25.5	0.625	−0.595	−6.8	−27.4	19.5	−0.22	
43.....	Gl 12	12.5 ± 0.9	2	12.10	49.6	0.618	0.319	−51.8	24.8	−29.4	−0.33	85/15

NOTES.—Col. (1), identifier from the PMSU1 tables; col. (2), pCNS3 name; col. (3), distance estimate and associated uncertainty—an uncertainty of ±0.0 km s^{-1} indicates $\epsilon_d < 0.1$ pc; col. (4), source of the distance estimate; col. (5), visual absolute magnitude; col. (6), radial velocity, usually from either PMSU3 or Delfosse et al. 1999, but see note to cols. (13) (the echelle data are accurate to ±1 km s^{-1}, while the low-resolution data are accurate to ±10 km s^{-1}); cols. (7) and (8), proper motion from either *Hipparcos* data (col. [4] = 1) or the pCNS3; cols. (9), (10), and (11), derived (U, V, W) space motions; col. (12), Hα equivalent width, where, following PMSU3, a negative value indicates absorption; col. (13), comments on individual stars: the relative weights of the trigonometric/spectroscopic parallax measurements contributing to d are given (see above), and "low-res." indicates that the star has no PMSU3 echelle observations and that both the Hα equivalent width and the radial velocity are from the PMSU1 low-resolution data. Table 2 is presented in its entirety in the electronic edition of the Astronomical Journal. A portion is shown here for guidance regarding its form and content.

REFERENCES.—(1) Trigonometric parallax from the *Hipparcos* Catalogue (ESA 1997). (2) PMSU1 (Reid et al. 1995). The relative weights given to trigonometric and spectroscopic parallax measurements are listed in col. (13); for example, 85/15 indicates that 85% of the weight rests with $\pi_{\rm trig}$. (3) Trigonometric parallax from the pCNS3 (Gliese & Jahreiss 1991).

A greater concern is the potential for kinematic bias. As discussed in PMSU1 and PMSU2, most stars in the pCNS3 were identified based on their having high proper motion. Those stars are drawn predominantly from three major proper-motion surveys: the Lowell survey, limited to $\mu > 0\farcs26$ yr^{-1} (Giclas, Burnham, & Thomas 1971); the Luyten half-second (LHS) catalog, $\mu > 0\farcs50$ yr^{-1} (Luyten 1979); and the new Luyten two-tenths (NLTT) catalog, $\mu > 0\farcs18$ yr^{-1} (Luyten 1980). Those limits correspond to transverse velocities of, respectively, 24.6, 47.4, and 17.1 km s^{-1} at 20 pc. Of the three surveys, the last has received the least attention. While Weis (1986, 1987, 1988) has obtained $(B)VRI$ photometry for many of the brighter ($m_r \leq 13.5$) red stars in the NLTT Catalogue, it is only recently that systematic attempts have been made to identify nearby stars among its fainter members (Reid & Cruz 2002; Salim & Gould 2002) Thus, there is a clear potential for bias against stars with low tangential motions in both the pCNS3 and the VC^2 sample.

We can test for kinematic bias by comparing the proper motions and transverse motions of the full VC^2 sample against similar data for the subset of stars that are included in the objective-prism surveys of Vyssotsky (1956) and Upgren et al. (1972). Since the latter stars were identified based on spectral type, that subsample should be free of any kinematic selection effects. Two hundred nine of the 448 systems in the VC^2 sample are in the Vyssotsky catalog, while the Upgren et al. survey contributes four systems.

Most of the spectroscopically selected stars are early-type M dwarfs, and those stars lie predominantly at larger distances in the VC^2 sample. This is illustrated in the top panels of Figure 4. Since the average distance of the spectroscopic subset is higher than the full sample, we must compare the tangential velocity distributions rather than the proper-

TABLE 3

BASIC DATA FOR SUPPLEMENTARY STARS

HIP	Name	Distance (pc)	M_V	V_r (km s^{-1})	μ_α (arcsec yr^{-1})	μ_δ (arcsec yr^{-1})	U (km s^{-1})	V (km s^{-1})	W (km s^{-1})	Hα (Å)
6290	LHS 1234	19.0 ± 1.9	8.97	22 ± 5[a]	−0.294	0.436	9.5	38.7	33.7	. . .
29052	LP 838-16	11.4 ± 0.3	11.58	. . .	−0.184	−0.204	8.0	−0.4	−12.5	Abs.
34361	GJ 2055	17.2 ± 0.7	9.93	. . .	0.195	−0.210	17.9	−13.7	6.3	Abs.
36985	G112-29	14.3 ± 0.3	9.09	. . .	0.036	−0.253	10.0	−12.9	−5.9	0.5
38594	Ross 429	19.5 ± 0.6	8.30	. . .	−0.300	0.200	−27.1	13.5	−14.0	Abs.
48659	LP 847-48	11.5 ± 0.4	11.74	. . .	−0.104	−0.154	0.7	−3.8	−9.3	0.3
55605	V130	16.1 ± 6.8	9.33	70 ± 20[b]	0.256	−0.147	13.1	−34.4	63.7	Abs.
56157	LP 672-42	14.0 ± 0.8	11.26	. . .	−0.355	0.262	−28.9	2.5	2.9	0.2
92444	CD −27°13268	17.3 ± 0.6	8.46	. . .	−0.140	−0.023	3.0	−6.1	9.4	. . .
103039	LP 816-60	5.5 ± 0.1	12.71	. . .	−0.307	0.031	4.9	0.3	6.3	. . .
105533	BD +10°4534	20.7 ± 0.7	8.33	. . .	−0.057	0.032	2.2	2.1	5.6	. . .
110980	LP 640-74	21.9 ± 0.9	8.81	. . .	0.045	−0.197	6.2	−15.9	−12.2	. . .
114242	HD 218422	19.9 ± 4.3	8.71	. . .	−0.087	−0.167	13.1	−11.8	1.8	. . .

NOTE.—Astrometric and photometric data are from the *Hipparcos* Catalogue. The Hα measurements are from unpublished spectroscopy with the CTIO 1.5 m telescope; as in Table 2, a positive equivalent width indicates emission.

[a] From Wilson 1953.

[b] From Evans 1979.

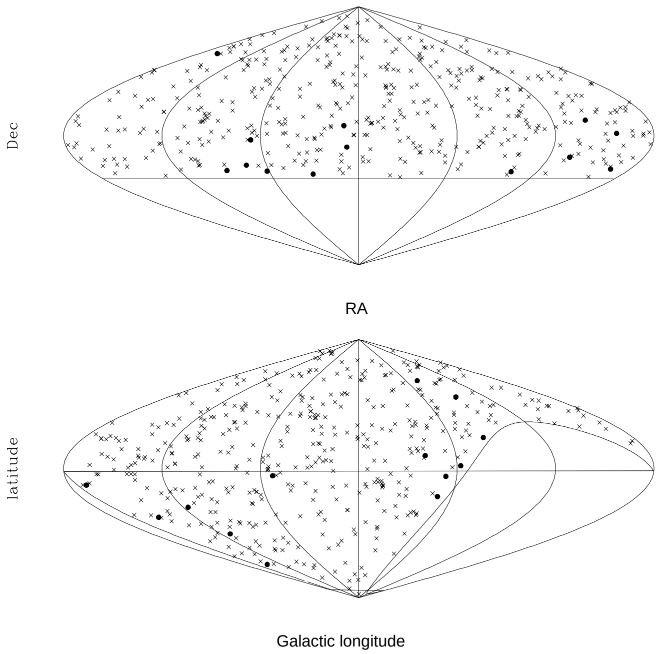

FIG. 3.—Distribution of the VC^2 systems on the celestial sphere, as a function of both equatorial and Galactic coordinates. The solid line indicates the $-30°$ limit in both cases.

motion distributions. That comparison is shown in the bottom panels of Figure 4, where the dotted line in the right panel marks the fractional contribution of the spectroscopic subset to the full sample. If there were a significant bias against stars with low transverse motions, we would expect the proportion of spectroscopically selected stars to rise with decreasing $V_{\rm tan}$. The data show little evidence of that effect. Dividing the distribution into two subsets, with $V_{\rm tan} \leq 20$ km s^{-1} and $V_{\rm tan} > 20$ km s^{-1}, the ratios $N_{\rm prism}/N_{\rm tot}$ are $44.0\% \pm 7.4\%$ and $48.6\% \pm 4.7\%$, respectively.

Our tests therefore reveal no evidence of significant bias in the VC^2 sample, either against stars lying within 10° of the Galactic plane or against stars with low tangential motions. On that basis, we conclude that the VC^2 sample provides a reliable data set for examining the space density and kinematics of the local Galactic disk population.

3. THE LUMINOSITY FUNCTION

3.1. *Space Densities*

We next consider how the revised distances obtained by *Hipparcos* affect the nearby-star luminosity function, $\Phi(M_V)$. We also take this opportunity to redetermine $\Phi(M_V)$ for earlier-type (BAFGK) main-sequence stars in the solar neighborhood, and to identify lower mass companions to those stars that should be added to the PMSU M dwarf statistics. Despite the availability of *Hipparcos* data for more than half a decade, many recent luminosity function analyses are still based on the statistics compiled by Wielen, Jahreiss, & Krüger (1983) from the Second Catalogue of Nearby Stars (CNS2; Gliese 1969) and its supplement (Gliese & Jahreiss 1979). An exception is the sample discussed by Kroupa (2001). Clearly, the systematics evident in Figure 1 have a significant influence on our estimate of the local density of main-sequence stars.

The *Hipparcos* Catalogue has a formal completeness limit of

$$V = 7.9 + 1.1 \sin|b| ,$$

so the 25 pc sample is effectively complete over the whole sky for $M_V \leq 5.9$. However, since the mission involved pointed observations of preselected targets, the survey includes a high proportion of stars known or suspected of being in the immediate solar neighborhood. Indeed, Jahreiss & Wielen (1997) argued that the *Hipparcos* Catalogue is essentially complete to $M_V = 8.5$ for stars within 25 pc of the Sun, providing a useful complement to the $8 < M_V \leq 16$ VC^2 sample.

We have identified 831 *Hipparcos* stars with $\pi_{\rm H} \geq 40$ mas and $M_V \leq 8.0$. Three issues need to be addressed before deriving a luminosity function from this data set: the evolutionary status of the individual stars, binarity and multiplicity, and the local intermixing of stellar populations. The first and last considerations are illustrated in Figure 5, which plots the $(M_V, B-V)$ color-magnitude diagram for all 1477 stars in the *Hipparcos* Catalogue with $\pi_{\rm H} \geq 40$ mas. Evolved stars clearly make a significant contribution at brighter magnitudes, and we have excluded them by eliminating stars that meet the following criteria:

$$M_V < 7.14(B-V) - 1.0 , \quad M_V < 5.0 .$$

This removes 41 stars from the sample.

Figure 5 includes a number of stars lying well below the disk main sequence. Most are fainter than $M_V = 8.0$ and are either white dwarfs, stars with substantial uncertainties in the measured parallax, or stars lacking $B-V$ colors. Four stars, however, lie just below the main sequence, with $6 < M_V < 8$. These are the halo subdwarfs HIP 18915 (HD 25329; [Fe/H] $= -1.6$), HIP 57939 (HD 103095; [Fe/H] $= -1.4$), HIP 67655 (HD 120559; [Fe/H] $= -0.94$), and HIP 79537 (HD 145417; [Fe/H] $= -1.25$). While the statistics are not overwhelming, a total of four subdwarfs in a sample of $\sim$650 FGK disk dwarfs implies a local number ratio of $\sim 0.6\% \pm 0.3\%$, a factor of 3 higher than the density normalization adopted for the halo in most Galactic structure analyses. All four stars are excluded from the present analysis.

Finally, we have checked SIMBAD for references to binary and multiple systems among the remaining 786 stars. Thirteen systems have wide companions listed separately in the *Hipparcos* database, while a further 213 have unresolved companions at small separations or wide companions that are not included in the *Hipparcos* data set. Where necessary, we have adjusted the photometry to allow for the contribution from fainter components, most notably in the case of HIP 66212 (HD 110836), which the uncorrected *Hipparcos* data place well above the main sequence. As illustrated in Figure 6, these corrections move a handful of primary stars to magnitudes fainter than $M_V = 8.0$.

Even after applying photometric adjustments, a small number of stars still lie well above the main sequence in Figure 6. Some (e.g., Gl 610) may be unrecognized binaries. Several, however, are primaries in binary systems (e.g., Gl 795A, GJ 1161A, Gl 118.2A), and the presence of the known secondary may affect either the photometry or the astrometry. Others are metal-rich stars (e.g., Gl 614, Gl 848.4, HD 217107, all known to harbor extrasolar planets),

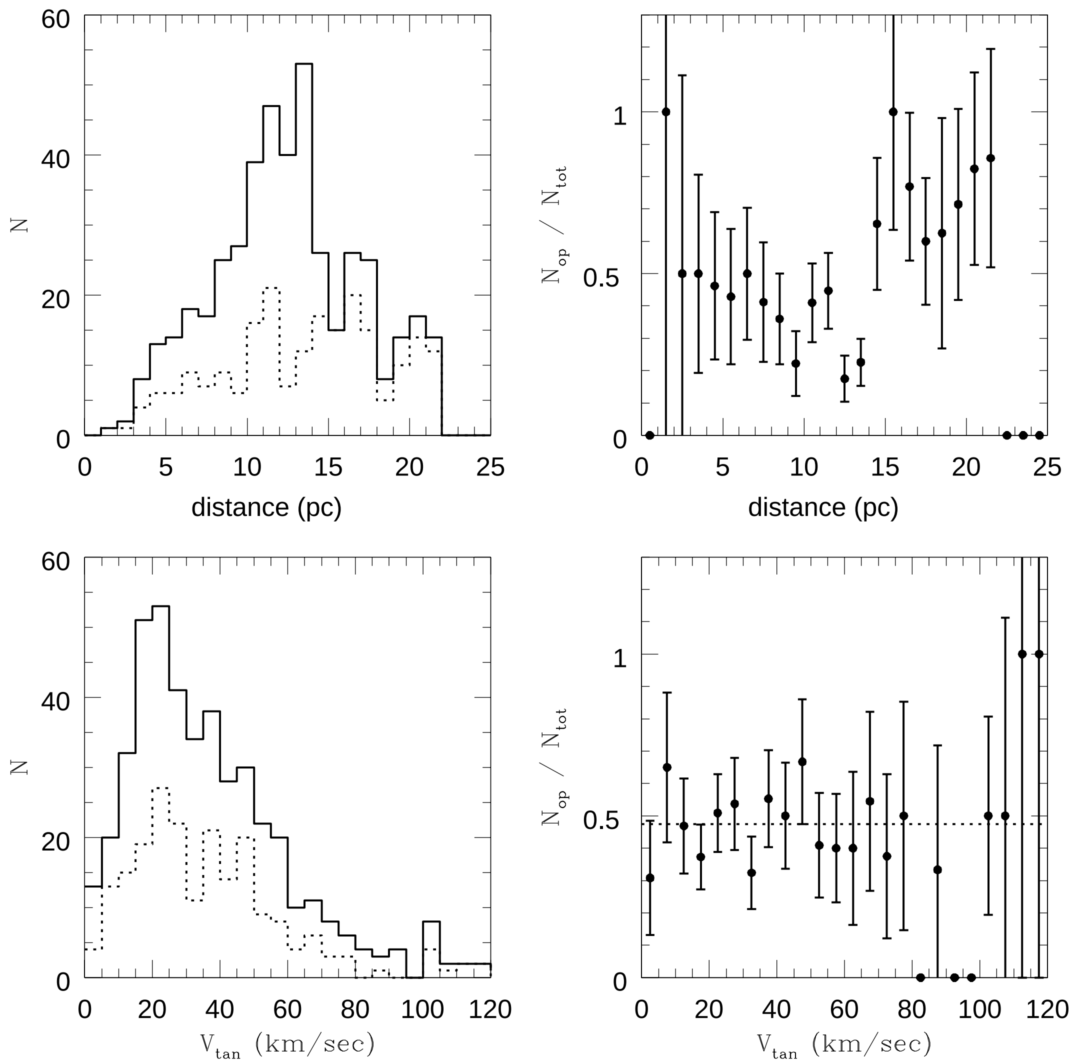

FIG. 4.—Comparison between the properties of the full VC[2] sample and the subset of stars identified in the Vyssotsky (1956) and Upgren et al. (1972) objective-prism surveys. The top panels plot the distribution as a function of distance: *left*, the differential number distribution, with the full sample plotted as a solid line and the spectroscopically identified subset as a dotted line; *right*, the fractional contribution from the spectroscopically selected sample. The predominant contribution of the latter at larger distances is clearly illustrated. The bottom panels plot the differential distribution as a function of tangential velocity, with the right panel plotting the fractional contribution from the spectroscopically selected sample. The horizontal dotted line in the latter panel indicates the fractional contribution of the latter stars to the full sample.

while still others, lying near the base of the subgiant branch, may be slightly evolved (e.g., Gl 19, Gl 368). Further spectroscopy and photometry are required to resolve these issues completely.

We noted above that the *Hipparcos* data set is expected to be effectively complete within 25 pc for stars with $M_V < 8.5$. We can test this hypothesis using the same techniques applied to the PMSU M dwarfs in § 2. Figure 7 plots the run of density with distance for systems in which the primary has M_V of 4.5 ± 0.5, 5.5 ± 0.5, 6.5 ± 0.5, and 7.5 ± 0.5. The first point marks the average density within a sphere, radius 16 pc, centered on the Sun; subsequent point plot the densities within annuli of radii 16–18, 18–20, 20–22, and 22–25 pc. Given Poisson uncertainties, there is no evidence of a significant decline in completeness as one approaches the 25 pc distance limit.

Our final sample includes 764 *Hipparcos* systems with $d < 25$ pc and $M_V < 8.0$. A further 12 binaries have primaries with $8 < M_V \leq 9$. Four of those stars are already included in the PMSU sample, while three stars lie beyond 22 pc (the PMSU distance limit appropriate to this absolute magnitude). The remaining five stars are added to the PMSU sample. We also extend coverage to $M_V \geq 16$ by adding data for the three systems currently known with $d < 5$ pc and $\delta > -30°$ (GJ 1111, Gl 406, LHS 292). Table 4 gives final statistics for the combined PMSU and *Hipparcos* 25 pc samples, and Figure 8 plots the composite luminosity function $\Phi(M_V)$.

We have compared our results against the luminosity function derived by Wielen et al. (1983). The space densities derived here are systematically lower than in the earlier study, reflecting the systematic errors present in pre-*Hipparcos* distance estimates. Kroupa (2001) finds similar results in his analysis. Overall, we derive a local number density of 0.106 main-sequence stars per cubic parsec, and a density of 0.0725 systems pc^{-3}. With evolved systems contributing a further 41 systems within 25 pc (6.3×10^{-4} pc^{-3}), the average separation between systems is $\sim$2.4 pc.

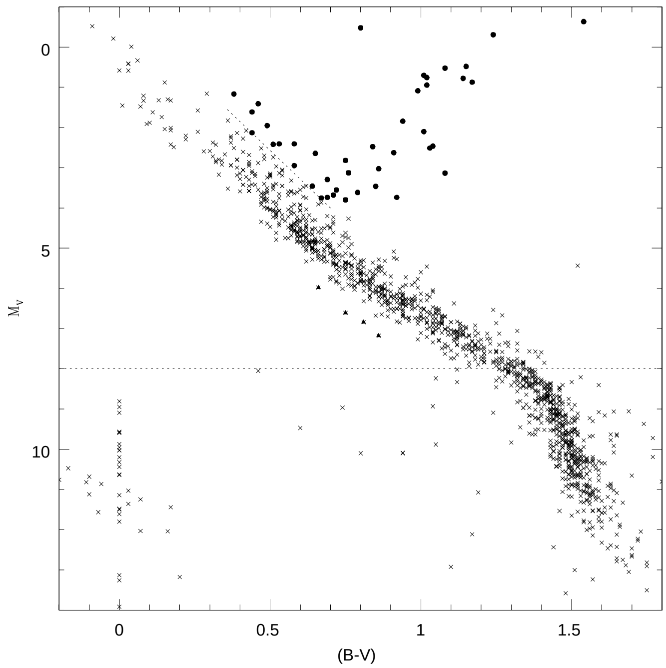

FIG. 5.—The (M_V, $B-V$) color-magnitude diagram for *Hipparcos* stars with $\pi > 40$ mas. The four subdwarfs discussed in the text are plotted as triangles, while stars identified as giants or subgiants are plotted as circles.

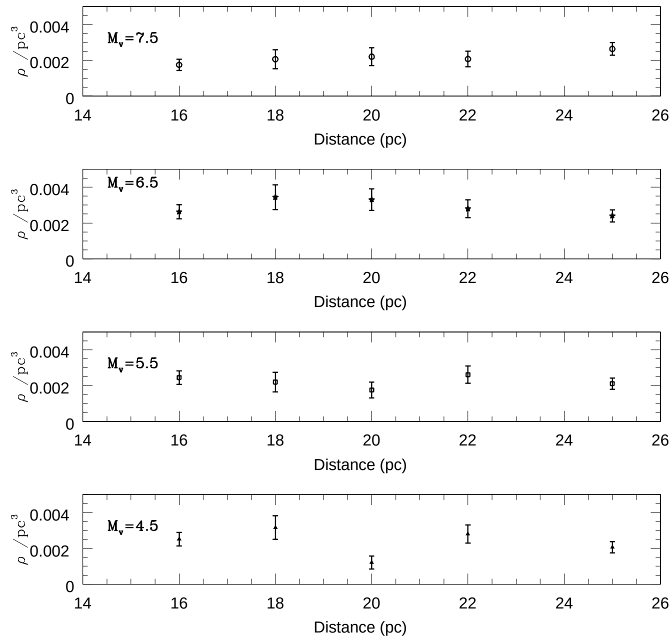

FIG. 7.—Run of density with distance for main-sequence stars with $4 < M_V < 8$. The initial point marks the mean density within 16 pc for each absolute magnitude interval; subsequent points plot the density within annuli from 16 to 18, 18 to 20, 20 to 22, and 22 to 25 pc. There is no evidence of a significant downturn with increasing distance, indicating a high degree of completeness in the sample.

3.2. *Binarity and Multiplicity*

The 764 systems in our *Hipparcos* 25 pc upper main-sequence sample include 538 single stars, 204 binaries (including eight low-amplitude spectroscopic binaries from Nidever et al. 2002), 22 triples, and four quadruple systems.

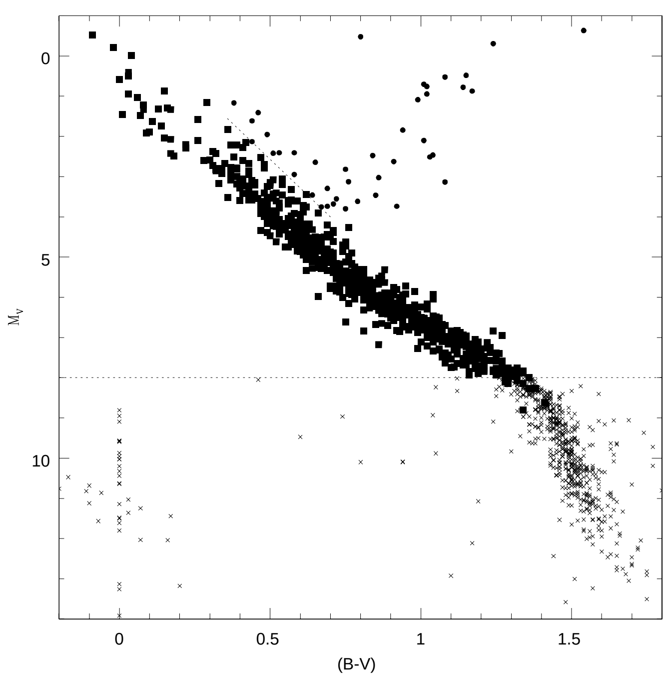

FIG. 6.—The (M_V, $B-V$) color-magnitude diagram after adjusting magnitudes of close binary systems to allow for the contribution from fainter components. Squares mark stars in our 25 pc sample; note that several fall below $M_V = 8$ after correction for binarity. Other symbols have the same meaning as in Fig. 5.

The resultant multiplicity fraction is only 30.1% $\pm$ 2.4%, somewhat lower than the value of 44% derived in the standard reference for this subject, Duquennoy & Mayor's (1991, hereafter DM91) analysis of observations of solar-type dwarfs. This discrepancy may reflect poorer observational coverage of the *Hipparcos* sample. Even with the addition of the extensive radial velocity data from the Lick/Keck planet-search survey, summarized by Nidever et al. (2002), 98 stars lack radial velocity measurements, and we noted in the previous section that a number of stars lie above the main sequence, suggesting unrecognized binarity.

An alternative possibility is that the multiplicity fraction measured for the 25 pc sample is more reliable than the DM91 statistics. The lower binarity might be a consequence of the larger magnitude range spanned by the present sample, since M dwarfs are known to have a lower fraction of stellar companions than do solar-type stars (Fischer & Marcy 1992; RG97). In addition, the improved parallax data lead to a better-defined sampling volume for the present data set than for the DM91 data set. We explore these issues here.

In analyzing the multiplicity of solar-type stars, Duquennoy & Mayor's intention was to define a volume-limited sample, including systems with spectral types between F7 and G9, declinations $\delta > -15^\circ$, and parallaxes exceeding 45 mas. However, since the parallaxes were drawn from the CNS2, they are subject to the systematic errors and potential biases illustrated in Figure 1. Fortunately, all of the DM91 stars are included in the *Hipparcos* Catalogue.

Figure 9 compares parallax data listed in the CNS2 against *Hipparcos* measurements for the DM91 reference sample. As expected, over 40% of the sample lie beyond the nominal 25 pc distance limit, including almost all stars with $B-V > 0.8$, most of which are subgiants. Only 102 systems

TABLE 4
THE NEARBY-STAR LUMINOSITY FUNCTION

M_V (1)	*Hipparcos* N_1 (2)	*Hipparcos* $N_{c,1}$ (3)	*Hipparcos* $N_{c,2}$ (4)	PMSU4 N_1 (5)	PMSU4 $N_{c,1}$ (6)	PMSU4 $N_{c,2}$ (7)	N_S (8)	Φ_1 (10^4 stars pc^{-3}) (9)	Φ_{tot} (10^4 stars pc^{-3}) (10)
−0.5 ...	3	...	...	...	...	...	...	0.46	0.46
0.5......	5	1	1	...	...	...	...	0.76	0.92
1.5......	15	2	2	...	...	...	...	2.29	2.60
2.5......	36	1	1	...	...	...	...	5.50	5.65
3.5......	79	9	9	...	...	...	...	12.07	13.45
4.5......	151	15	15	...	...	...	...	23.07	25.36
5.5......	147	19	19	...	...	...	...	22.46	25.36
6.5......	181	32	32	...	...	...	...	27.65	32.54
7.5......	143	24	24	...	...	...	...	21.85	25.52
8.5......	8	41	27	103	7	7	6	32.01	40.16
9.5......	...	23	13	92	7	5	3	50.21	58.26
10.5	...	28	4	64	15	9	...	74.24	88.16
11.5	...	21	2	66	17	11	3	76.56	91.06
12.5	...	15	6	71	25	17	1	82.36	107.30
13.5	...	7	...	23	14	6	...	73.21	92.31
14.5	...	...	...	13	6	3	...	41.38	50.93
15.5	...	5	1	4	12	5	...	101.86	248.28
16.5	...	...	...	1	2	2	...	25.46	76.39
17.5	...	...	...	2	6	1	...	50.93	76.39

NOTES.—Col. (2), number-magnitude distribution of single stars and primary stars in the *Hipparcos* 25 pc sample; col. (3), magnitude distribution for all known companions; col. (4), number of companions that fall within the distance limits given in Table 1; cols. (5)–(7), same as cols. (2)–(4) for the PMSU4 sample; col. (8), contribution from the supplementary stars listed in Table 3; col. (9), the luminosity function due to primaries and single stars in the combined samples; col. (10), space densities including the contribution from the companions listed in cols. (4) and (7).

have $\pi_H \geq 45$ mas. However, of those 102 systems, 42 are double or multiple, giving a multiplicity fraction of 41% ± 7%, consistent with the value of 44% derived for the full data set in DM91. Observational bias in the DM91 sample is therefore not likely to be responsible for the discrepancy with respect to the *Hipparcos* 25 pc sample.

Even with the extensive temporal coverage and high accuracy provided by the CORAVEL radial velocity observations, it is likely that a significant number of binary systems remain unrecognized among the DM91 G dwarf sample. Binary systems with high inclination, long period, or both have low velocity amplitudes and are, therefore, more diffi-

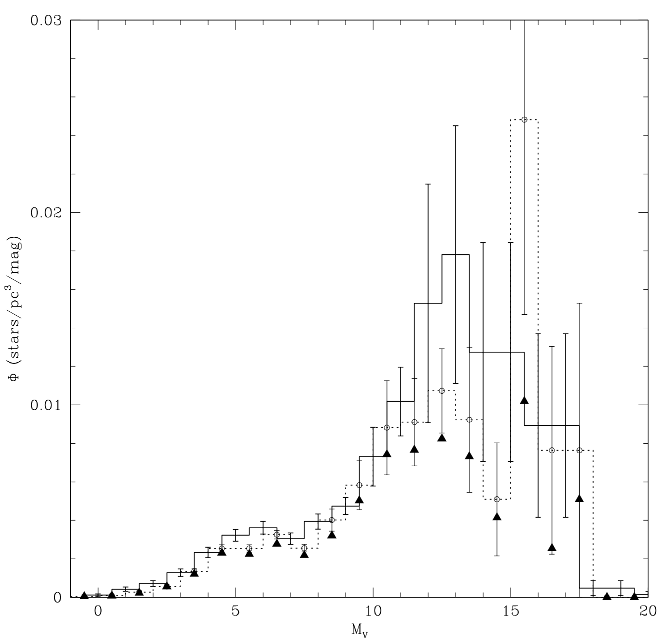

FIG. 8.—Luminosity function for nearby stars, derived by combining data for the *Hipparcos* 25 pc sample and the PMSU sample. Data for single stars and primaries are plotted as triangles; the circles plot the space densities once the appropriate companions are included, with the error bars reflecting Poisson uncertainties. The solid histogram plots $\Phi(M_V)$ from Wielen et al. (1983).

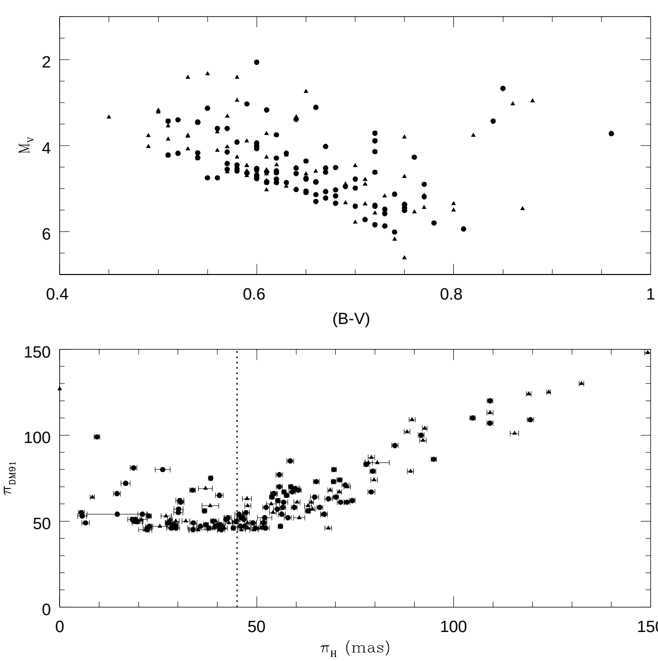

FIG. 9.—Duquennoy & Mayor G dwarf sample: *bottom*, comparison of the parallaxes listed in the CNS2 against the *Hipparcos* data; *top*, distribution of the stars in the (M_V, $B-V$)-plane. Single stars are plotted as triangles, binaries as circles. The photometry of the latter stars has been corrected to exclude contributions from secondary components.

cult to detect. Duquennoy & Mayor concluded that their analysis might underestimate the binary fraction among G dwarfs by approximately one-third, implying a true multiplicity close to 60%. On the other hand, 47 of the 60 "single" stars in the $\pi_H \geq 45$ mas DM91 subsample are included in the Lick/Keck planet-search program: 46 are classed as having stable radial velocities ($\sigma_V < 0.1$ km s^{-1}); only HIP 98819 (Gl 779) is identified as a confirmed spectroscopic binary (Nidever et al. 2002).

Based on these results, we take 60% as a likely upper limit for the multiplicity of the upper main-sequence stars in the *Hipparcos* 25 pc sample. Given the relatively sparse observational scrutiny, we assume that the known secondaries are characteristic of the sample as a whole, and we therefore allow for potential "missing" binary companions by giving double weight to known binary components in the statistical analysis. Figure 10 shows the resultant effect on $\Phi(M_V)$: the space densities are still systematically lower than the Wielen et al. (1983) values. The overall space density becomes 0.112 stars pc^{-3}.

4. THE MASS FUNCTION

4.1. *The Mass-Luminosity Relation*

The mass-luminosity relation is a key ingredient in transforming the stellar luminosity function to a mass function. Since we have only *BV* data for most of the stars in the present sample, we require a relation between mass and M_V. In general, masses can be derived only for stars in binary systems (gravitational lensing offers the potential for deriving accurate masses for single stars, but it requires particular source-lens geometries). Henry & McCarthy (1993) provided the first extensive analysis of lower main-sequence astrometric binaries. They derive a three-segment fit in the (M_V, log (mass))-plane, extending from 2 $M_\odot$ to the hydrogen burning limit. Together with their mass-M_K and mass-$M_{\rm bol}$ relations, this calibration has served as the primary reference over the last decade.

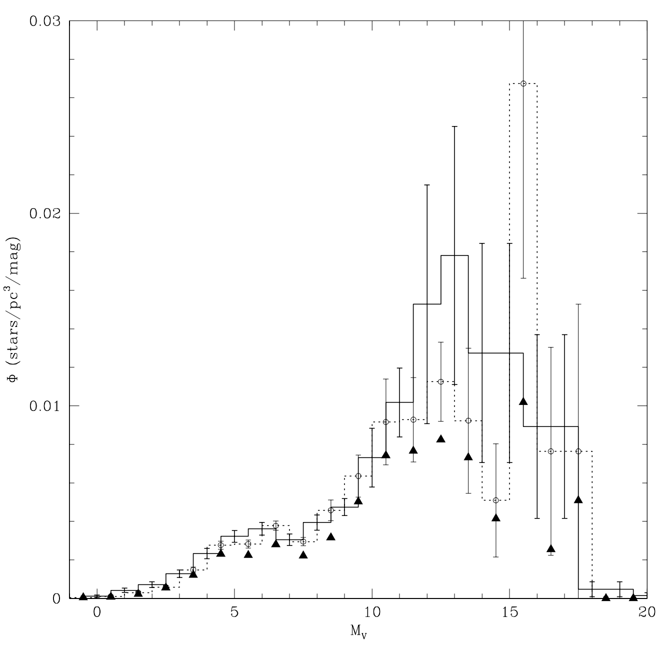

FIG. 10.—The nearby-star luminosity function, adjusted to include the contribution from "missing" binary components. The symbols have the same meaning as in Fig. 8. As discussed in the text, we have doubled the contribution from known companions to the *Hipparcos* 25 pc sample.

Most recent attention has centered on low-mass stars, with the addition of new data from high-precision *Hubble Space Telescope* (Henry et al. 1999) and ground-based astrometry, and from high-accuracy radial velocity measurements (Delfosse et al. 1999; Ségransan et al. 2000). Delfosse et al. (2000, hereafter D00) have used these new observations to derive a revised mass-M_V relation for lower main-sequence stars,

$$\log M = 10^{-3} \times (0.3 + 1.87M_V + 7.614M_V^2 - 1.698M_V^3 + 0.06096M_V^4) .$$

As Figure 11 shows, this relation predicts higher masses by 10%–15% than Henry & McCarthy's calibration for $11 < M_V < 15$.

Delfosse et al. limit their analysis to M dwarfs, and Henry & McCarthy's piecewise mass-M_V relation extends only to 2 $M_\odot$, but the *Hipparcos* 25 pc sample includes more massive A- and B-type stars. We have therefore used the data compiled by Andersen (1991) for eclipsing binary systems to derive an empirical mass-M_V relation covering the upper main sequence. That relation is

$$\log M = 0.477 - 0.135M_V + 1.228 \times 10^{-2}M_V^2 - 6.734 \times 10^{-4}M_V^3 ,$$

and it is plotted in Figure 11. We combine that relation with the D00 result, setting the boundary between the two calibrations at $M_V = 10.0$, where the agreement is better than 5%.

In addition to these empirical calibrations, Kroupa, Tout, & Gilmore (1993, hereafter KTG) derived a semiempirical mass-M_V relation. Adopting the Wielen et al. (1983) luminosity function as a reference, they represented the mass function as a three-component power law and vary the indices to minimize residuals in the mass-M_V relation. Figure 11 compares their derived relation against the empirical results. The KTG calibration, spanning absolute magnitudes between $M_V = +2$ and $M_V = +17$, matches the D00 relation at low masses and lies up to 8% below the empirical relation (i.e., predicts lower masses at a given M_V) for solar-mass stars.

4.2. *The Present-Day Mass Function*

We have computed present-day mass functions using both the D00 empirical calibration and the KTG semiempirical relation, extending both to higher masses using our fit to the Andersen (1991) eclipsing binary data set. Figure 12 shows the results derived from the empirical calibration. Defining

$$\xi(M) = \frac{dN}{d \log M} , \quad \psi(M) = \frac{dN}{dM} ,$$

the top panel plots $\xi(M)$ for the *Hipparcos* 25 pc and the PMSU samples [i.e., the data set used to construct $\Phi(M_V)$ in Fig. 8]. The dotted histogram shows the mass function derived from single stars and primaries in multiple systems. The middle panel in Figure 12 plots $\xi_{2B}(M)$, where double weight is given to the *Hipparcos* 25 pc secondary components (i.e., the data set used to construct Fig. 10). Adding

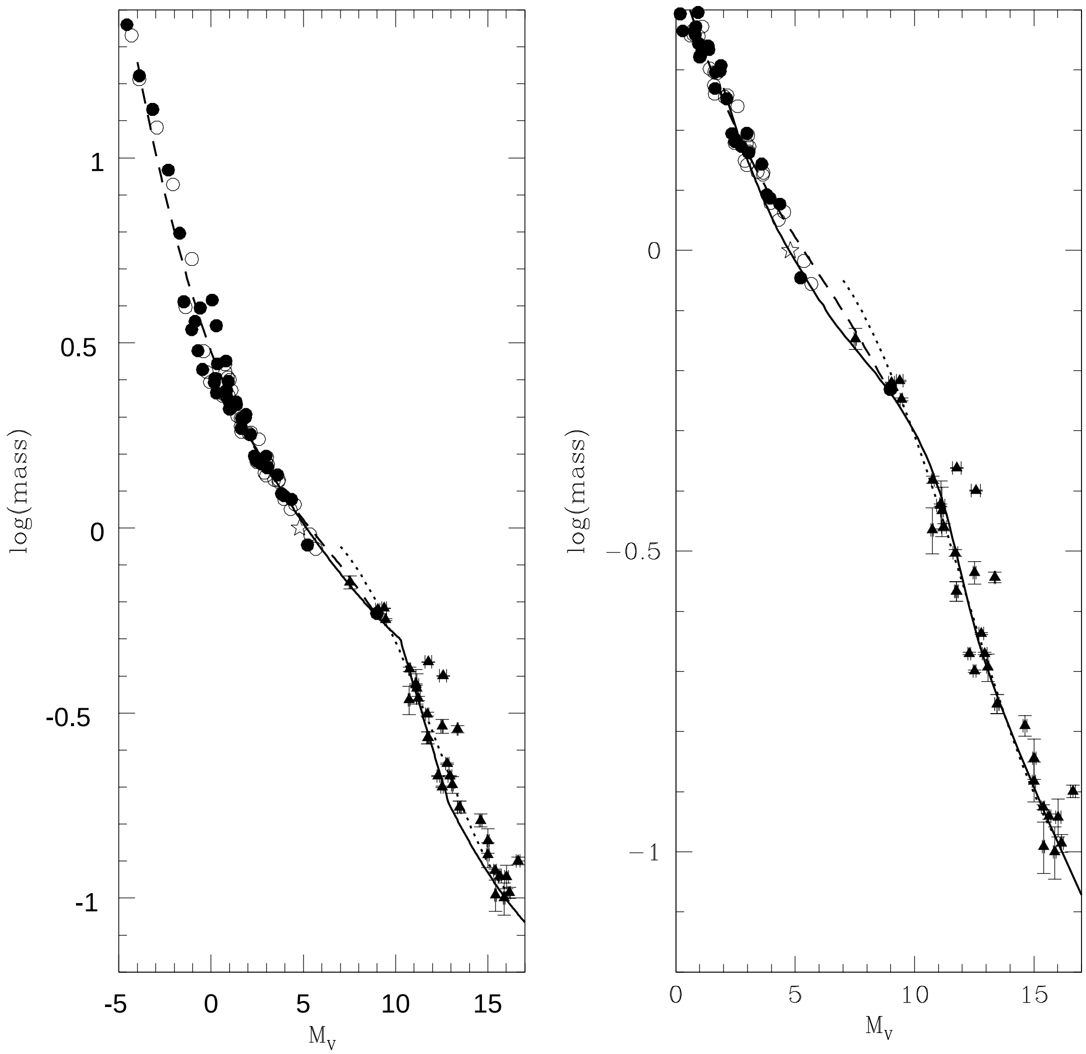

FIG. 11.—The mass-M_V relation for main-sequence stars. Filled and open circles plot data for primary and secondary stars, respectively, from Andersen's (1991) compilation of eclipsing binaries; triangles plot data for lower main-sequence binaries from Ségransan et al. (2000). The five-pointed star marks the Sun. In the left panel, the dashed line shows the empirical fit to the upper main-sequence stars given in the text, the dotted line plots the mass-M_V relation derived by Delfosse et al. (2000), and the solid line shows the three-component fit from Henry & McCarthy (1993). The right panel compares the former two relations against the Kroupa et al. (1993) semiempirical relation (*solid line*).

the hypothetical as yet undiscovered binaries produces little change in the overall morphology. Integrating the mass functions, we derive a local mass density of $\rho_{\rm MS} = 0.0310$ $M_\odot$ pc^{-3} from $\xi(M)$ and 0.0338 $M_\odot$ pc^{-3} when double weight is given to the secondaries in the *Hipparcos* sample. We note that white dwarfs contribute a further 0.004 $M_\odot$ pc^{-3} (RG97).

We have also used the empirical mass-M_V relation to recompute the mass function derived from the northern ($\delta \geq -30°$) 8 pc sample. The original sample from RG97 has been updated to take into account *Hipparcos* parallax data and new stellar companions (Reid et al. 1999, hereafter R99). Chabrier & Baraffe (2000) and Kroupa (2001) have suggested that this sample provides unreliable statistics, both through the inclusion of stars whose distances rest on photometric or spectroscopic parallax estimators and through incompleteness. Neither objection is valid. As emphasized in R99, 100 of the 104 systems have accurate ($\epsilon < 10\%$) trigonometric parallax measurements, while only a handful of additions have been identified since 1997. The most recent is 2MASS J1835379+325954, an M8 dwarf at 5.7 pc, in Reid et al. (2002a). As discussed in that paper, the over 30% deficit in number density between the 8 pc and extrapolated 5 pc sample (Henry et al. 1997) includes a substantial contribution from bright ($M_V < 14$) stars and probably overestimates the shortfall by at least a factor of 2.

The mass function derived from the 8 pc sample is plotted in the bottom panel of Figure 12. Again, the single-star/primary mass function is plotted as a dotted histogram. Below 1 $M_\odot$, the results are statistically identical to those based on the composite *Hipparcos* 25 pc/PMSU analysis (i.e., employing a 5 pc limit at $M_V > 15$). The total mass density derived by integrating $\xi_8(M)$ is 0.0288 $M_\odot$ pc^{-3}, the lower value reflecting the relative scarcity of G dwarfs within 8 pc of the Sun.[4]

[4] We note that the 2 σ deficit of G dwarfs in a comparison of the 8 pc and 25 pc samples has the same statistical weight as the 2 σ excess of $M_V = 16$ stars in a comparison between the 5 pc and 8 pc samples. There appears to be little concern, however, over " missing " G dwarfs within 8 pc of the Sun.

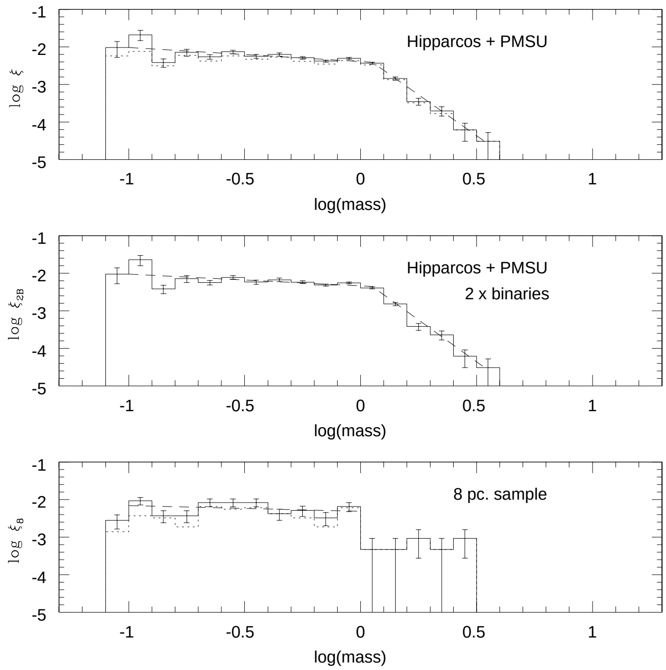

FIG. 12.—Stellar mass function for the solar neighborhood: *top*, results of applying the mass-luminosity relation to the data set used to derive $\Phi(M_V)$, plotted in Fig. 8, with the dotted histogram outlining the contribution from single stars and primary stars in binary systems; *middle*, $\xi(M)$ when double weight is given to the *Hipparcos* 25 pc secondaries; *bottom*, $\xi(M)$ for the northern 8 pc sample (Reid et al. 1999). In each case, the dashed lines plot the best-fit power law (see text).

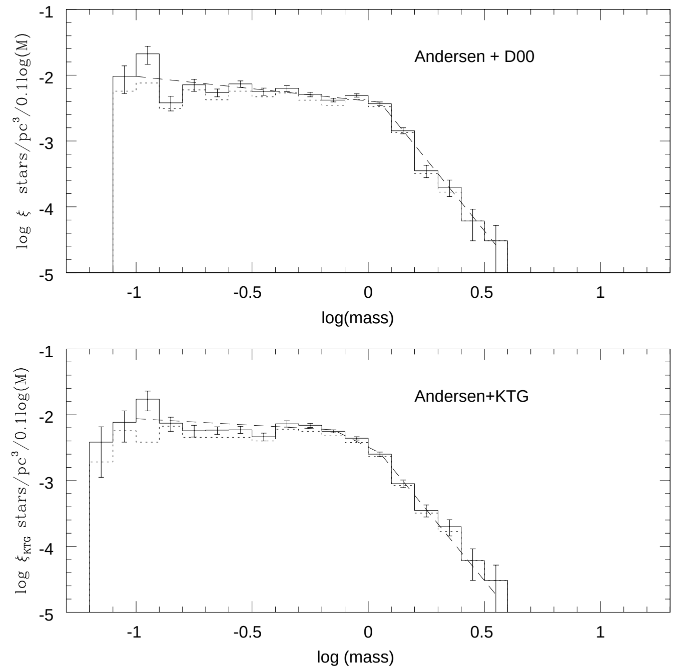

FIG. 13.—Comparison between the present-day mass function derived using the empirical mass-M_V calibration (*top*) and the Kroupa et al. (1993) semiempirical calibration (*bottom*). The latter includes the empirical eclipsing binary relation for $M_V < 3.5$. As in Fig. 12, the dotted histogram plots results for single stars and primaries. The main differences lie at near-solar masses, with the semiempirical calibration showing a steepening at $\sim$0.7 $M_\odot$ rather than $\sim$1 $M_\odot$.

Following Salpeter (1955), it is convenient to represent the mass function as a power law,

$$\xi(M) = M^{-\alpha+1} , \quad \psi(M) = M^{-\alpha} ,$$

where $\alpha = 2.35$ is the Salpeter slope. The mass functions plotted in Figure 12 are all well represented by a two-component power law. Both *Hipparcos*/PMSU analyses are consistent with $\alpha = 1.35 \pm 0.2$ for $0.1\ M_\odot < M < 1\ M_\odot$ and $\alpha = 5.2 \pm 0.4$ for $M > 1\ M_\odot$. The steep slope at masses above 1 $M_\odot$ emphasizes the fact that $\xi(M)$ is the present-day mass function (Miller & Scalo 1979); our calculations take no account of higher mass stars that have evolved off the main sequence over the lifetime of the Galactic disk. The 8 pc sample has fewer high-mass stars than the *Hipparcos* data set, but it still shows a clear break near 1 $M_\odot$, and we derive $\alpha = 1.15 \pm 0.2$ for $0.1\ M_\odot < M < 1\ M_\odot$, matching the original RG97 analysis. In each case, fitting to the single-star/primary data set flattens the distribution below 1 $M_\odot$, yielding $\alpha \sim 1$, since secondaries make a proportionately higher contribution at lower masses.

Figure 13 compares results from the empirical and semiempirical mass-M_V calibrations. The derived mass functions are in broad agreement, particularly at low masses. As might be expected from Figure 11, the main differences arise at near-solar masses. Rather than a single break at $\sim$1 $M_\odot$, the semiempirical relation produces changes in slope at $\sim$0.7 and $\sim$1.1 $M_\odot$ (masses close to the break points chosen by KTG in their calibration procedure).

Fitting $\xi_{\rm KTG}(M)$ as a combination of power laws, we find $\alpha = 1.3 \pm 0.15$ for $0.1\ M_\odot < M < 0.7\ M_\odot$ (fitting $0.15\ M_\odot < M < 0.7\ M_\odot$ gives $\alpha = 1.03 \pm 0.11$), $\alpha = 2.8 \pm 0.4$ for $0.7\ M_\odot < M < 1.1\ M_\odot$, and $\alpha = 4.8 \pm 0.15$ for $M > 1.1\ M_\odot$. Not unexpectedly, these results are very similar to those derived by Kroupa (2001). Integrating over the mass function, we find that main-sequence stars contribute 0.0300 $M_\odot$ pc^{-3} to the local mass density. As with the empirical calibration, allowing for additional binaries among the *Hipparcos* 25 pc sample increases $\rho_{\rm MS}$ by $\sim$10%.

Comparing $\xi(M)$ and $\xi_{\rm KTG}(M)$, the main difference is the steepening of the latter between $\sim$0.7 and 1.0 $M_\odot$, reflecting the differences in the mass-M_V relations evident in Figure 11. Additional calibrating binaries in this mass range would clearly be very useful. That discrepancy apart, there is considerable similarity between the global properties of the two present-day mass functions plotted in Figure 13: $\alpha \sim 1.2$ at low masses, $\alpha \sim 5$ at supersolar masses, and, depending on the binary fraction, an integrated mass density of 0.030–0.034 $M_\odot$ pc^{-3}.

4.3. *The Initial Mass Function*

The observed mass function, $\xi(M)/\psi(M)$, specifies the relative number of main-sequence stars as a function of mass in the local Galactic disk at the present time. A more fundamental quantity is the initial mass function, denoted here as $\Xi(M)$ (logarithmic mass units) or $\Psi(M)$, the relative number of stars forming as a function of mass. Three factors need to be taken into account in converting the present-day mass function to the initial mass function: stellar evolution, the density distribution perpendicular to the plane, and the local mix of stellar populations.

Salpeter (1955) originally pointed out the necessity of allowing for evolution beyond the main sequence in computations of the "original mass function." M dwarfs have main-sequence lifetimes $\tau_{\rm MS}$ well in excess of 20 Gyr, so $\xi(M)$ includes low-mass stars spanning the full history of star formation in the disk. Higher mass stars have shorter hydrogen-burning lifetimes, and $\xi(M)$ only takes account of stars with ages $\tau < \tau_{\rm MS}$. Thus, the present-day census includes only a fraction of the total population if $\tau_{\rm MS}$ is less than the age of the Galactic disk, $\tau_{\rm disk}$. Correcting the observed numbers for this effect requires that we estimate the age of the disk and adopt a stellar birthrate as a function of time.

Binney, Dehnen, & Bertelli (2000) summarize the various techniques that have been used to estimate the age of the local disk population. Those include analyses of the low-luminosity cutoff in the disk white dwarf luminosity function, measurements of isotopic ratios, isochrone matching for individual stars, and quantitative analysis of the distribution of stars in the Hertzsprung-Russell diagram. Individual age estimates range from 7 to 15 Gyr; we adopt $\tau_{\rm disk} = 10$ Gyr in the present calculations. Following the discussion in PMSU3, we assume a constant star formation rate, so the correction factor is given by

$$f_{\rm MS} = \tau_{\rm disk}/\tau_{\rm MS} \quad \text{for} \quad \tau_{\rm MS} < \tau_{\rm disk} \; .$$

These corrections are applied on a star-by-star basis to the *Hipparcos* sample, with the appropriate main-sequence lifetimes computed from

$$\log \tau_{\rm MS} = 1.015 - 3.491 \log M + 0.8157 (\log M)^2 \; .$$

This relation is derived from the solar abundance models computed by Schaller et al. (1992).

The decrease in main-sequence lifetime with increasing mass also requires accounting for the vertical density distribution, $\rho(z)$. Velocity dispersion increases with age, so the younger average age of higher mass stars leads to lower velocities and a density distribution that is confined more closely to the plane. Thus, a local volume-limited sample of the latter stars, drawn from near the Galactic midplane, includes a larger fraction of the total population.

We correct for this effect following Miller & Scalo (1979). The vertical density distribution of disk stars can be represented by an exponential distribution, scale height z_0. Most recent studies derive a value of $z_0 \sim 250$ pc for long-lived main-sequence stars ($M_V > 4$); younger upper main-sequence stars, $M_V < 3$, have lower velocity dispersions and a steeper density distribution, $z_0 \sim 100$ pc (Haywood, Robin, & Crézé 1997; Siegel et al. 2002). We adopt a scale height of 170 pc for stars with intermediate absolute magnitudes, $3 < M_V < 4$. Deriving accurate estimates of surface density from $\psi(M)$ is a complex operation, requiring modeling of the overall potential (see, e.g., Kuijken & Gilmore 1989). We assume that the effective surface densities Σ scale linearly with z_0,

$$\Sigma \propto \rho_0 z_0 \; ,$$

where ρ_0 are the volume densities plotted in Figures 12 and 13.

Finally, since we aim to derive $\Xi(M)$ for the disk, we need to take account of solar neighborhood stars that are members of other stellar populations. For present purposes, we consider three components: disk, thick disk, and halo (stellar, not dark matter). While the last component makes a negligible contribution locally (§ 3.1), approximately 10% of the stars in the immediate solar neighborhood are part of the more extended thick disk (see § 5.2). The full characteristics of the latter population, particularly the abundance and age distribution, remain uncertain, but star counts at $z > 1000$ pc demonstrate there are few, if any, stars younger than a few gigayears, and that the vertical density distribution has a scale height 3–4 times that of $M_V > 4$ disk stars (Siegel et al. 2002). Given those results, we assume that 90% of local stars with $M_V \geq 4$ are disk dwarfs and scale $\psi(M)$ accordingly.

Figure 14 shows the initial mass functions derived from $\xi(M)$ and $\xi_{\rm KTG}(M)$; both data sets are based on the observed *Hipparcos* 25 pc and PMSU samples (i.e., we have not applied corrections for potential undetected secondary components). In both cases, $\Xi(M)$ can be represented as a two-component power law: with the empirical mass-M_V relation, the data are consistent with $\alpha = 1.3 \pm 0.2$ at $M < 1.1\ M_\odot$ and $\alpha = 2.8 \pm 0.25$ at higher masses; adopting the semiempirical mass-M_V relation yields $\alpha = 1.1 \pm 0.15$ at $M < 0.6\ M_\odot$ and $\alpha = 2.5 \pm 0.15$ at higher masses, consistent with results derived by Kroupa (2001). Reducing the assumed age of the disk to 8 Gyr steepens α at high masses by $\sim$0.15; increasing $\tau_{\rm disk}$ to 12 Gyr flattens α to a similar extent.

4.4. *Modeling $\Xi(M)$: Power Laws or Lognormal Functions?*

Power laws provide a mathematically simple means of representing the stellar initial mass function and give an adequate match to the data plotted in Figure 14. Some recent studies, however, find that mass functions of this form are less successful in matching data for young clusters

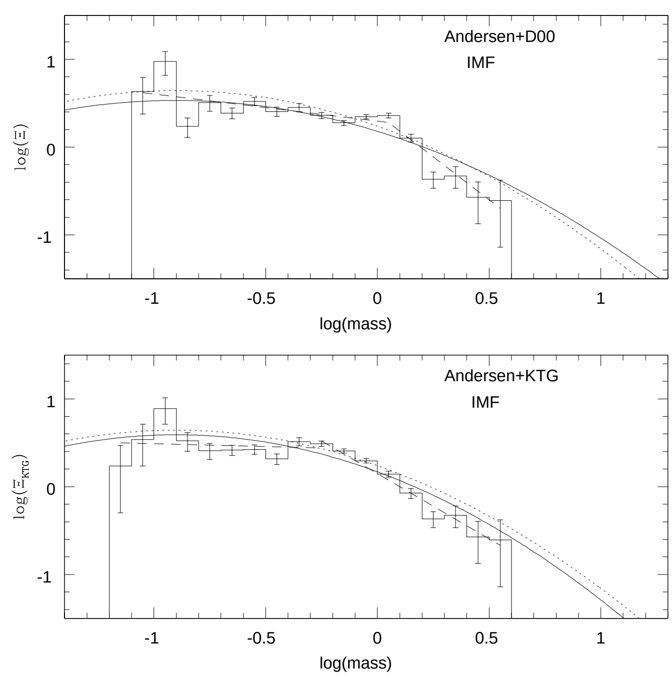

FIG. 14.—The initial mass function: *top*, results based on the empirical mass-M_V relation; *bottom*, results using the Kroupa et al. (1993) semiempirical relation at $M_V > 3.5$. The units on the ordinate axis are surface density, with an arbitrary normalization. The dashed lines mark the power-law representations described in the text. The solid line and dotted line plot log-normal functions, with the former plotting the best-fit function (see text) and the latter the original Miller-Scalo function with $C_1 = 1.15$.

and associations. In particular, Hillenbrand & Carpenter (2000) find that $\psi(M)$ peaks at $\sim 0.15\ M_\odot$ in the central regions of the Orion Nebula cluster.[5] Miller & Scalo (1979) provided an alternative to power laws in their lognormal representation of the initial mass function,

$$\Xi(M) = C_0 \exp\left[-C_1(\log M - C_2)^2\right] ,$$

where C_0, C_1, and C_2 are constants defining the normalization, width, and maximum of the initial mass function.

The main impact of adopting a lognormal representation of $\Xi(M)$ is twofold: first, the existence of a preferred mass (10^{C_2}) has implications for star formation models; second, the extrapolation below the hydrogen burning limit affects expectations of the frequency of brown dwarfs. Neither of the initial mass functions plotted in Figure 14 extends to substellar masses. Measuring $\Psi(M)$ at those masses in the field is complicated severely by the rapid luminosity evolution of brown dwarfs, as discussed in R99. Modeling the mass function as a power law, R99 found that a simple extension of the low-mass stellar initial mass function ($\alpha = 1.3 \pm 0.3$) provides a reasonable match to the (still scarce) observations. Chabrier (2002) arrives at similar conclusions. However, the field brown dwarf sample is likely to be dominated by longer lived, higher mass objects, $M > 0.04\ M_\odot$. As Figure 14 shows, within those limits (0.04–0.08 $M_\odot$), there is relatively little difference in slope between the Miller-Scalo functions and an $\alpha \sim 1$ power law. More extensive observations of young clusters, and improved models for pre–main-sequence dwarfs, still offer the best prospects of establishing $\Psi(M)$ at these low masses.

We have matched lognormal distributions against the observations. We have fixed $C_2 = -0.9$ and defined a goodness-of-fit statistic,

$$\chi^2_\nu = \frac{1}{\nu}\sum\frac{(O-C)^2}{\epsilon^2} ,$$

where O and C are the observed and predicted values of $\Xi(M)$, ϵ is the associated Poisson uncertainty, and $\nu = n_{\rm bin} - 2$. We allow both C_0 and C_1 to vary. The best-fit results are $C_1 = 1.0$ for $\Xi(M)$ and $C_1 = 1.2$ for $\Xi_{\rm KTG}(M)$ (the values of C_0 have no physical significance, since our density scaling has an arbitrary zero point). These results are plotted in Figure 14, together with the best-fit match for $C_1 = 1.15$, the original value derived by Miller & Scalo (1979). The χ^2_ν-values for those fits are 8.34 and 6.08, respectively (for $\nu = n_{\rm bin} - 3$); in comparison, the power-law representation yields $\chi^2_\nu = 4.34$ and $\chi^2_\nu = 4.66$, respectively.

In summary, lognormal Miller-Scalo functions provide a poorer representation of the overall shape of the derived initial mass functions than simple power-law fits. Having noted that, one should bear in mind the caveat that the differences between the two "observed" functions plotted in Figure 14 highlight the continued potential for systematic effects introduced by changes in the mass-luminosity relation. Nonetheless, the main challenge facing star formation theory appears to lie in providing an explanation for the change in power-law index between 0.7 and 1.1 $M_\odot$.

[5] We note that Luhman et al. (2000), using a different set of evolutionary tracks, find that the mass function of the Orion Nebula cluster is consistent with a power law, $\alpha \sim 1$, to $\sim 0.04\ M_\odot$.

5. GALACTIC DISK KINEMATICS

In PMSU1, we used our observations of the VC sample to study the motions of local stars, and in PMSU2 we examined the different kinematics exhibited by M dwarfs with and without detectable Hα emission. Those analyses were based on radial velocities derived from the intermediate-resolution spectra used to measure band strengths and determine spectral types. We can reexamine those issues using the more accurate distances and radial velocities measured for the VC^2 sample.

5.1. *Solar Motion and the Schwarzschild Velocity Ellipsoids*

We have used standard techniques (Murray 1983) to parameterize the kinematics of the M dwarfs in the VC^2 sample. We calculate the solar motion and Schwarzschild ellipsoid parameters for (U, V, W) Galactic coordinates, where U is positive toward the Galactic center, V is positive in the direction of rotation, and W is positive toward the north Galactic pole. This matches the coordinate system used in the pCNS3.

This standard calculation measures the velocity distributions of stars within a small spherical volume, centered on the Sun and lying near the midpoint of the Galactic plane. Wielen (1974, 1977) has argued that weighting the velocity dispersion by the W-velocity (effectively, the inverse residence time in the plane) provides a more useful estimator. Those dispersions are calculated as follows:

$$\sigma_U^2 = \frac{\sum_i |W_i| U_i^2}{\sum_i |W_i|}, \quad \sigma_V^2 = \frac{\sum_i |W_i| V_i^2}{\sum_i |W_i|} ,$$
$$\sigma_W^2 = \frac{1}{2}\frac{\sum_i |W_i| W_i^2}{\sum_i |W_i|} .$$

Both sets of velocity dispersions are listed in Table 5, together with the mean velocity relative to the Sun, the solar motion. The results are consistent both with our previous studies, based on lower-accuracy radial velocities, and with other analyses of nearby-star samples (e.g., Dehnen & Binney 1998).

As in PMSU2, we have segregated M dwarfs in the VC^2 sample with measurable Hα emission. In the PMSU2 analysis, the low-resolution spectroscopy limited this sample to stars with equivalent widths exceeding 1.0 Å; in the present sample, with the higher resolution PMSU3 echelle data, the effective limit is 0.1 Å. Eighty-three stars in the VC^2 sample meet this criterion, and the resulting mean kinematics are listed in Table 5. As discussed in PMSU2, Hα emission declines with increasing age, so it is no surprise that the unweighted velocity dispersions are significantly lower than those of the full VC^2 sample. In contrast, the weighted velocity dispersions are markedly higher. This reflects the influence of a small number of stars with large W-velocities (e.g., GJ 1054, $W = -95.3$ km s^{-1}, and Gl 630.1, or CM Dra, $W = -83$ km s^{-1}) and illustrates the vulnerability of this calculation to small number statistics.

We have also determined the mean kinematics for stars in the *Hipparcos* 25 pc sample. As noted above, 98 of the 764 systems in this sample lack radial velocities, and those stars are not included in our statistics. Most of the latter systems have low proper motions, as one might expect given their pre-*Hipparcos* obscurity: 74 ($\sim$75%) have $\mu < 0\farcs3$ yr^{-1}, and 73 have $V_{\rm tan} < 30$ km s^{-1}. Ignoring those stars in the present

TABLE 5
KINEMATICS OF NEARBY STARS

Sample	N	$\langle U \rangle$ (km s^{-1})	$\langle V \rangle$ (km s^{-1})	$\langle W \rangle$ (km s^{-1})	σ_U (km s^{-1})	σ_V (km s^{-1})	σ_W (km s^{-1})	Note
VC^2 dM + dMe......	436	−9.7	−22.4	−8.9	37.9	26.1	20.5	Unweighted
					42.1	32.9	32.2	$\|W\|$-weighted
					34	18	16	Core
VC^2 dMe................	83	−15.4	−16.5	−10.1	25.0	21.1	17.8	Unweighted
					33.6	44.6	36.1	$\|W\|$-weighted
					12	11	11	Core
Hipparcos $M_V < 4$...	137	−7.8	−10.0	−8.9	27.4	14.2	14.2	Unweighted
					29.4	15.4	21.8	$\|W\|$-weighted
					35	18	16	Core
Hipparcos $M_V \geq 4$...	532	−12.7	−22.8	−6.5	39.9	27.9	19.1	Unweighted
					45.2	33.4	29.2	$\|W\|$-weighted
					26	14	10	Core

NOTES.—Unweighted: $\sigma = \sum [(x_i - \bar{x})/n]$. $|W|$-weighted: weighted using Wielen's prescription (see text). Core: linear fit to central regions of probability distributions (Fig. 16).

analysis may affect the derived (U, V, W) distributions at low velocities, although the comparisons in the following section suggest that this is not a severe effect.

We have divided the *Hipparcos* data set into two subsamples: 138 systems with $M_V < 4$ (137 with V_r measurements), and 626 systems with $M_V \geq 4$ (528 with radial velocities). Table 5 lists the mean kinematics of those data sets, and Figure 15 compares the (V, U) and (W, U) velocity distributions against data for the VC^2 sample. The fainter *Hipparcos* stars are kinematically indistinguishable from the M dwarf sample, as one would expect, given that both data sets should sample the same underlying population—disk dwarfs with ages spanning the star formation history of the Galactic disk. The brighter *Hipparcos* stars have significantly lower velocity dispersions than even the dMe sample, reflecting the short main-sequence lifetimes and younger ages of these more luminous stars. The derived kinematics for those stars are consistent with recent studies.

5.2. *The M Dwarf Velocity Distribution and the Thick Disk*

The rms velocity dispersions derived in the previous section provide a one-parameter characterization of the velocity distribution in each component. While useful as a simple means of comparing different stellar samples, that parameterization can be misleading if the underlying velocity distribution is non-Gaussian in nature. Probability plots (Lutz & Upgren 1980) provide a method of examining the velocity distributions in more detail: if a given sample is drawn from a Gaussian distribution, plotting the cumulative distribution in units of the measured rms dispersion yields a straight line.

Figure 16 shows (U, V, W) probability plots for the full VC^2 sample, the dMe stars from that sample, and both subsets of the *Hipparcos* data set ($M_V \geq 4$ and $M_V < 4$). The full VC^2 data set and the fainter *Hipparcos* sample have very similar velocity distributions, suggesting that even though the latter sample is not complete, the subset of stars with measured radial velocities is unbiased. The brighter *Hipparcos* stars and the dMe dwarfs, samples dominated by younger stars, have velocity distributions closest to those expected for Gaussian dispersions, although both, particularly the emission-line stars, become nonlinear at extreme velocities. A number of the higher velocity dMe dwarfs are known to be close binaries (e.g., CM Dra). These stars could be older systems, where tidal locking maintains enhanced rotational velocities and stronger Hα emission.

All four data sets exhibit near-linear distributions at low velocities, suggesting that each includes a core subset of stars with Gaussian velocity distributions. We have measured the slope of the central regions for each distribution. In U and W, the gradients are derived for the range $-1 < \sigma < 1$; the V-distributions become nonlinear more rapidly at negative velocities (lagging the solar rotational velocity), and we fit the slope in the range $-0.5 < \sigma < 2$. The resulting measurements are listed in Table 5.

We propose that the linear core in these probability distributions represents the disk population in each sample. The two younger data sets, the brighter *Hipparcos* stars and the dMe dwarfs, have been subjected to less secular scattering and, therefore, have lower velocity dispersions. The nonlinearities are more pronounced at large $|\sigma|$ in the other two samples and, in at least U and W, are symmetric, suggesting the presence of a second, higher velocity dispersion component. The obvious candidate for the latter is the thick disk. Identified originally by Gilmore & Reid (1983), the thick disk is evident as a flattening of the density law, $\rho(z)$, at ~1–1.5 kpc above the plane. Initial analyses of $\rho(z)$ suggested a low local density normalization [$\rho_{TD}(z = 0) \sim 0.02\rho_{\rm disk}(z = 0)$] and high scale height (>1.3 kpc), but more recent studies (Haywood et al. 1997; Siegel et al. 2002) favor a higher normalization (~5%) and a smaller scale height (0.7–1 kpc). Its origin remains uncertain, but as noted in the previous section, the scarcity of main-sequence A and F stars indicates $\tau > 3$ Gyr. There are no direct, unbiased measurements of the abundance distribution.

The rotational properties of the thick disk are not yet well established, complicating analysis of the V velocity distributions. However, we do not expect a significant solar motion in either U or W, while a stellar component with a larger scale height must also have a higher σ_W than disk dwarfs. Modeling the latter velocity distributions should therefore provide insight into both thick disk kinematics and the local density normalization.

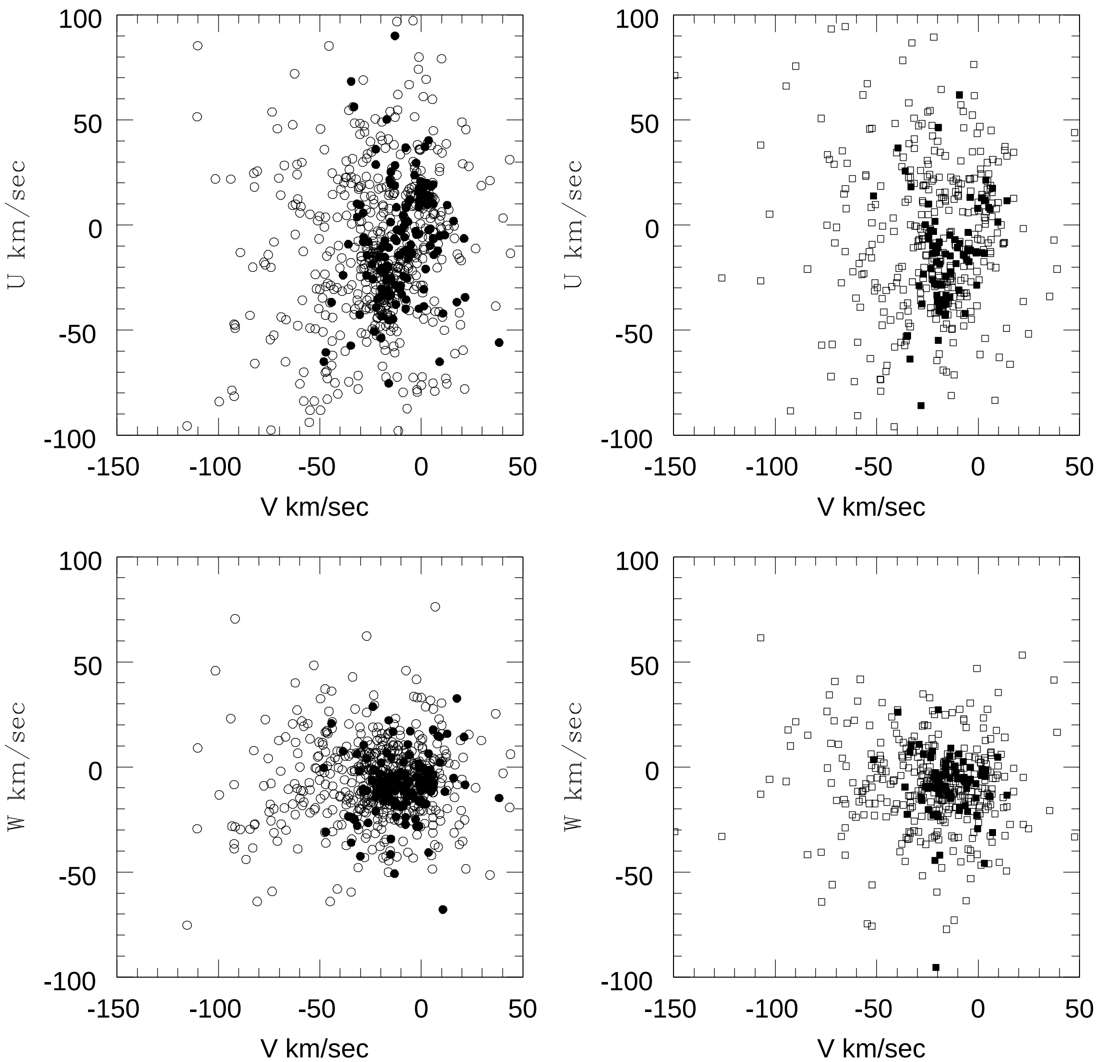

FIG. 15.—The (U, V, W) diagrams for the VC^2 (*right*) and *Hipparcos* 25 pc (*left*) data sets. Filled points mark dMe dwarfs in the VC^2 sample and *Hipparcos* stars with $M_V < 4.0$, respectively.

We have matched the observed W-velocity probability distributions of the VC^2 and faint *Hipparcos* samples against models derived by combining two Gaussian components (σ_1 and σ_2) with a relative normalization, $f = N_1/N_2$. We set $\sigma_1 = 16$ km s^{-1}, matching the core of the observed distribution, and define the mean velocity as $W = -8$ km s^{-1} (VC^2) and -6 km s^{-1} (*Hipparcos*). We let σ_2 vary from 18 to 60 km s^{-1} in steps of 2 km s^{-1}, varying f between 0.02 and 0.20 at each velocity. At each step, we compute the rms residuals

$$R_s = \sum (W_i - W_c)^2 \ ,$$

where W_i is the observed velocity and W_c the predicted velocity for the measured σ_i (the abscissa in the probability plots). The quantity R_s is computed for the range $-2.5 < \sigma_i < 2.5$ to minimize the effect of outliers in the observed velocity distribution.

Matched against the models, both data sets exhibit a broad minimum in R_s centered at $\sigma_2 \sim 36$ km s^{-1} and $f \sim 0.12$. There is reasonable agreement between the model and the data for 34 km s$^{-1} < \sigma_2 < 48$ km s^{-1} and $0.1 < f < 0.2$ for the VC^2 sample, and for 34 km s$^{-1} < \sigma_2 < 42$ km s^{-1} and $0.1 < f < 0.16$ for the *Hipparcos* data set. In general, σ_2 and f are anticorrelated in those solutions. Figure 17 illustrates several examples. None of the models provide a good match to the data at $|\sigma| > 2.5$, where small number statistics can affect the observed distribution.

Analyzing the U velocity distribution gives similar results. Setting $\sigma_1 = 34$ km s^{-1} and matching the distribution for $|\sigma| < 2.5$, the best-fit values are $\sigma_2 = 60$–64 km s^{-1} and $f = 0.1$–0.12 for the VC^2 sample, and $\sigma_2 = 64$–70 km s^{-1} and $f = 0.1$–0.14 for the *Hipparcos* data set. Both data sets are consistent with approximately 10% of solar neighborhood stars being members of the higher velocity component.

Summarizing these results, a two-component Gaussian distribution with velocity dispersions $\sigma_1 = 16$ km s^{-1}, $\sigma_2 \sim 36$ km s^{-1}, and $f = 0.12$ provides a good representation of the observed W velocity distribution of solar neighborhood disk dwarfs. A two-component Gaussian with $\sigma_1 = 34$ km s^{-1}, $\sigma_2 \sim 62$ km s^{-1}, and $f = 0.12$ matches the

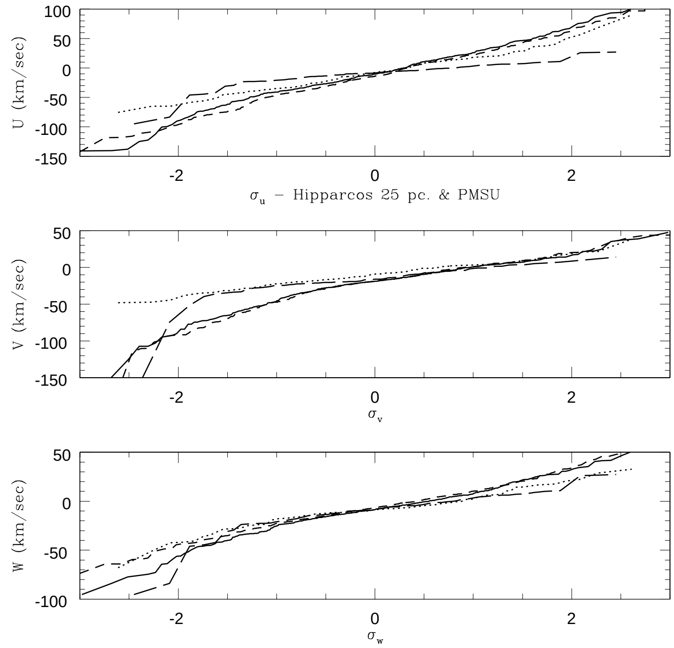

FIG. 16.—Probability plots for (U, V, W) velocity distributions. The solid lines plot data for the full VC^2 sample, the long-dashed lines outline data for the 83 dmE dwarfs in the VC^2 sample, and the dotted lines plot the distributions of the *Hipparcos* faint ($M_V > 4$) sample; the short-dashed lines plot the bright ($M_V \leq 4$) *Hipparcos* data set. The similarity between the full VC^2 and faint *Hipparcos* data sets is clear.

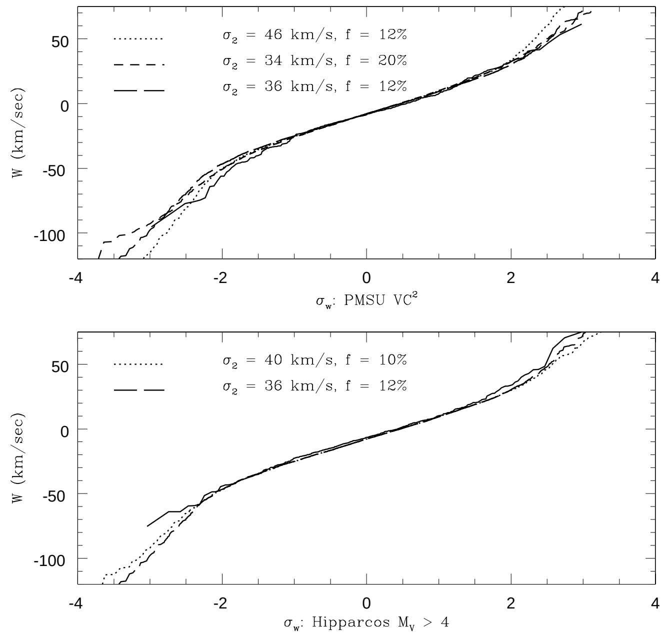

FIG. 17.—Two-component fits to probability plots of the W velocity distribution of the PMSU VC^2 M dwarf sample (*top*) and the *Hipparcos* faint-star sample (*bottom*). In both cases, the observations are plotted as a solid line and the low-velocity component is modeled with $\sigma_W = 16$ km s^{-1}; the tabulated velocity distributions and relative normalizations refer to the higher velocity component.

observations in U. In both U and W, approximately 10% of the sample resides in the higher velocity dispersion component. Given the results from recent star-count analyses, it seems reasonable to identify the latter stars as the local constituents of the thick disk.

5.3. *Ultracool M Dwarfs and the Thick Disk*

Reid et al. (2002b) have recently presented high-resolution echelle observations of a photometrically selected sample of ultracool M dwarfs (spectral types later than M7). One of the surprising results from that study concerns the velocity distributions, which have more similarity to our analysis of dMe dwarfs than to the kinematics of the full VC^2 sample. This is unexpected, since almost all ultracool M dwarfs are expected to be hydrogen-burning stars, albeit with masses very close to the hydrogen burning limit. With main-sequence lifetimes exceeding 10^{12} yr, ultracool dwarfs, like earlier-type M dwarfs, should span the full age range of the Galactic disk. One would expect such stars to have experienced a similar history of dynamical interactions, leading to kinematics matching the full VC^2 sample rather than the younger emission-line dwarfs.

A possible resolution to this dilemma lies with the two-component model. The observed velocity dispersions of the ultracool dwarfs are

$$(\sigma_U, \sigma_V, \sigma_W) = (32, 17, 17) \text{ km s}^{-1} .$$

These values are close to the velocity dispersions that we measure for the core of both the VC^2 and faint *Hipparcos* samples (Table 5). We have identified those core velocity dispersions as characteristic of the Galactic disk. Are the ultracool dwarfs essentially a pure disk sample?

There are two possible explanations for the absence of thick disk dwarfs in the ultracool sample. First, the result may be due to small number statistics: there are only 37 dwarfs in the photometrically selected sample analyzed in Reid et al. (2002b), implying an expected number of 4 ± 2 thick disk dwarfs. Alternatively, a systematic difference in metallicity could lead to thick disk stars' being intrinsically rarer among low-temperature, late-type dwarfs.

Expanding on the latter possibility, the location of the hydrogen burning limit in the Hertzsprung-Russell diagram is known to be a function of metallicity. This is illustrated most dramatically for extreme halo subdwarfs (e.g., NGC 6397; Bedin et al. 2001), where the main sequence terminates at ($M_V \sim 15$, $V-I \sim 3$), brighter and bluer than for the Galactic disk population. While the metal hydride absorption bands in those stars are consistent with late-type M dwarfs, the TiO absorption is closer to that observed in M3 dwarfs (Gizis 1997). This behavior is relevant because there are suggestions that the thick disk, as an old population, may have a mean metallicity $\langle[\mathrm{Fe/H}]\rangle < -0.4$ dex. This might be sufficient to move the hydrogen burning limit to an effective spectral type of ~M7, significantly reducing the contribution of thick disk dwarfs to an ultracool sample, without necessarily requiring a significant change in the underlying mass function.

We can test this hypothesis to a limited extent using data for the VC^2 sample. All of these stars have low-resolution spectroscopic observations, obtained as part of the PMSU survey. CaH and TiO band indices derived from those data can be used to provide a crude assessment of the metallicity

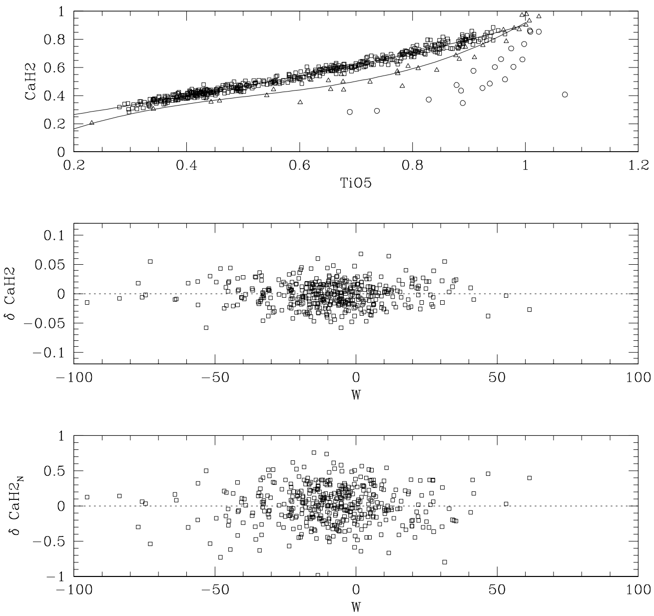

FIG. 18.—*Top*: CaH2/TiO5 distribution of the VC^2 M dwarfs (*squares*), intermediate subdwarfs (sdM, *triangles*), and extreme subdwarfs (esdM, *circles*). The solid lines are polynomial relations matched to the first two data sets. *Middle*: CaH2 residuals for the VC^2 dwarfs as a function of *W*-velocity. *Bottom*: Those residuals normalized to the offset between the mean M dwarf and sdM relations. Neither of the residual plots shows evidence of a systematic trend with velocity.

distribution. Figure 18 plots band strengths for the M dwarfs in the VC^2 sample and for nearby intermediate (sdM, [Fe/H] ~ -1) and extreme (esdM, [Fe/H] < -1.5) subdwarfs from Gizis (1997). We fitted mean relations to the VC^2 stars,

$$\langle \mathrm{CaH2} \rangle = 0.128 + 0.714\,\mathrm{TiO5} - 0.205\,\mathrm{TiO5}^2 + 0.266\,\mathrm{TiO5}^3 ,$$

and the intermediate subdwarfs,

$$\mathrm{CaH2}_{\mathrm{sdM}} = -\,0.219 + 2.632\,\mathrm{TiO5} - 4.149\,\mathrm{TiO5}^2 + 2.656\,\mathrm{TiO5}^3 .$$

The middle panel plots the raw residuals,

$$\delta\mathrm{CaH2} = \mathrm{CaH2}_{\mathrm{obs}} - \langle \mathrm{CaH2} \rangle ,$$

as a function of *W*-velocity; the bottom panel plots the normalized residuals,

$$\delta\mathrm{CaH2}_N = (\mathrm{CaH2}_{\mathrm{obs}} - \langle \mathrm{CaH2} \rangle)/(\mathrm{CaH2}_{\mathrm{sdM}} - \langle \mathrm{CaH2} \rangle) .$$

If thick disk dwarfs have systematically lower metallicities than disk dwarfs, one might expect a systematic trend in the residuals with increasing velocity. There is no evidence of such behavior in these data. However, the uncertainties in the abundance calibration are obviously substantial and could well obscure systematics at the expected level of $\sim$0.4 dex. A similar analysis of a volume-complete sample of G dwarfs, where abundances can be derived to higher accuracy, would be instructive.

6. CONCLUSIONS

In the first paper of this series (PMSU1), we used spectroscopic observations of stars in the pCNS3 to define a volume-limited sample of M dwarfs with absolute magnitudes in the range $8 < M_V \leq 14$, the VC sample. In the present paper, we have examined the effects of using *Hipparcos* distance estimates and adding newly discovered M dwarfs that meet the relevant distance limits. The revised sample, the VC^2 sample, includes 548 main-sequence stars in 448 systems and shows no evidence of systematic bias against stars with low space motions.

Using the revised sample, we have recomputed the stellar luminosity function $\Phi(M_V)$. We have combined those measurements with *Hipparcos* data for brighter stars within 25 pc of the Sun to derive the luminosity function for main-sequence stars with $-1 < M_V \leq 17$, making explicit allowance for potential unseen binary companions. The results are in good agreement with Kroupa's (2001) analysis for $M_V < 10$, but we derive lower space densities for mid- and late-type M dwarfs.

We have transformed the observed luminosity function to a mass function using both empirical and semiempirical mass-M_V calibrations, with the latter taken from Kroupa et al. (1993). The resulting present-day mass functions are in broad agreement, consistent with power-law distributions with $\alpha \sim 1.2$ at low masses ($M < 0.6\ M_\odot$) and $\alpha \sim 5$ at high masses ($M > 1.1\ M_\odot$). The semiempirical mass-M_V relation leads to a steepening in $\psi(M)$ ($\alpha \sim 2.2$ for $0.6\ M_\odot < M < 1.1\ M_\odot$). Data for additional binary stars with masses in the range $0.8\ M_\odot < M < 1.2\ M_\odot$ would be useful in resolving this discrepancy. However, there is little impact on the mass density derived by integrating $\psi(M)$; both analyses indicate that main-sequence stars contribute 0.030–0.033 $M_\odot$ pc^{-3} to the total mass density in the solar neighborhood.

We have converted the observed present-day mass function to estimates of the initial mass function by allowing for stellar evolution effects at high masses, and by integrating the density distribution perpendicular to the plane. We also apply a 10% correction to allow for the presence of thick disk dwarfs in the local sample. The derived initial mass functions have a near-Salpeter slope at high masses, $\alpha \sim 2.5$–2.8, but are relatively flat at low masses, $\alpha \sim 1.1$–1.3.

We also considered the kinematics of solar neighborhood stars. Analysis shows that both the M dwarfs in the VC^2 sample and the fainter stars ($4 < M_V \leq 8$) in the *Hipparcos* 25 pc data set have similar velocity distributions. This is not unexpected, since both should include representatives from the full star formation history of the Galactic disk. Both the brighter *Hipparcos* stars and the dMe dwarfs among the VC^2 sample have cooler kinematics, as expected for data sets with younger average ages. Detailed analysis of the *U* and *W* velocity distributions for the two older samples shows that both are well represented by two-component Gaussians, with approximately 10% of the stars in the higher velocity component. We identify the latter as the local component of the thick disk. A comparable analysis of a well-defined sample of solar-type stars offers the potential of obtaining insight into the detailed properties of this Galactic component.

Finally, we suggest that the thick disk component may provide an explanation for the surprisingly low velocity dispersions measured for a photometrically selected sample of ultracool dwarfs: If the thick disk is slightly metal-poor, the hydrogen burning limit could lie close to the M7 boundary of the ultracool sample. As a result, the coolest M dwarfs may represent a pure disk sample, a conclusion supported by the agreement between their kinematics and the core velocity dispersions measured for the FGK and early-/mid-type M dwarfs in our analysis.

This research was partially supported by a grant under the NASA/NSF "NStars" initiative, administered by the Jet Propulsion Laboratory, Pasadena. We have made extensive use of the SIMBAD database, operated at CDS, Strasbourg, France, and of the ADS bibliographic service.

REFERENCES

Andersen, J. 1991, A&A Rev., 3, 91
Bedin, L. R., Anderson, J., King, I. R., & Piotto, G. 2001, ApJ, 560, L75
Beuzit, J.-L., et al. 2001, A&A, submitted (astro-ph/0106277)
Binney, J., Dehnen, W., & Bertelli, G. 2000, MNRAS, 318, 658
Chabrier, G. 2002, ApJ, 567, 304
Chabrier, G., & Baraffe, I. 2000, ARA&A, 38, 337
Dehnen, W., & Binney, J. J. 1998, MNRAS, 298, 387
Delfosse, X., Forveille, T., Beuzit, J.-L., Udry, S., Mayor, M., & Perrier, C. 1999, A&A, 344, 897
Delfosse, X., Forveille, T., Ségransan, D., Beuzit, J.-L., Udry, S., Perrier, C., & Mayor, M. 2000, A&A, 364, 217 (D00)
Duquennoy, A., & Mayor, M. 1991, A&A, 248, 485 (DM91)
ESA. 1997, The Hipparcos and Tycho Catalogues (ESA SP-1200) (Noordwijk: ESA)
Evans, D. S. 1979, Interim Supplement to the General Catalogue of Stellar Radial Velocities (NSSDC/ADC Cat. 3047B) (Greenbelt, MD: GSFC)
Fabricius, C., & Makarov, V. V. 2000, A&AS, 144, 45
Fischer, D. A., & Marcy, G. W. 1992, ApJ, 396, 178
Giclas, H. L., Burnham, R., & Thomas, N. G. 1971, Lowell Proper Motion Survey, Northern Hemisphere (Flagstaff: Lowell Obs.)
Gilmore, G. F., & Reid, N. 1983, MNRAS, 202, 1025
Gizis, J. E. 1997, AJ, 113, 806
Gizis, J. E., Reid, I. N., & Hawley, S. L. 2002, AJ, 123, 3356 (PMSU3)
Gliese, W. 1969, Veröff. Astron. Rechen-Inst. Heidelberg, No. 22 (CNS2)
Gliese, W., & Jahreiss, H. 1979, A&AS, 38, 423
———. 1991, Preliminary Version of the Third Catalogue of Nearby Stars (NSSDC/ADC Cat. 5070A) (Greenbelt, MD: GSFC) (pCNS3)
Hawley, S. L., Gizis, J. E., & Reid, I. N. 1996, AJ, 112, 2799 (erratum 113, 1458 [1997]) (PMSU2)
———. 1997, The Palomar/MSU Nearby Star Spectroscopic Survey (NSSDC/ADC Cat. 3198) (Greenbelt, MD: GSFC)
Haywood, M., Robin, A. C., & Crézé, M. 1997, A&A, 320, 440
Henry, T. J., Franz, O. G., Wasserman, L. H., Benedict, G. F., Shelus, P. J., Ianna, P. A., Kirkpatrick, J. D., & McCarthy, D. W., Jr. 1999, ApJ, 512, 864
Henry, T. J., Ianna, P. A., Kirkpatrick, J. D., & Jahreiss, H. 1997, AJ, 114, 388
Henry, T. J., & McCarthy, D. W., Jr. 1993, AJ, 106, 773
Hillenbrand, L. A., & Carpenter, J. M. 2000, ApJ, 540, 236
Jahreiss, H., & Wielen, R. 1997, in *Hipparcos* Venice '97, ed. B. Battrick (ESA SP-402) (Noordwijk: ESA), 675
Kroupa, P. 2001, MNRAS, 322, 231
Kroupa, P., Tout, C. A., & Gilmore, G. 1993, MNRAS, 262, 545 (KTG)
Kuijken, K., & Gilmore, G. 1989, MNRAS, 239, 605
Luhman, K. L., Rieke, G. H., Young, E. T., Cotera, A. S., Chen, H., Rieke, M. J., Schneider, G., & Thompson, R. I. 2000, ApJ, 540, 1016
Lutz, T. E., & Upgren A. R. 1980, AJ, 85, 1390
Luyten, W. J. 1979, LHS Catalogue (2d ed.; Minneapolis: Univ. Minnesota)
———. 1980, NLTT Catalogue (Minneapolis: Univ. Minnesota)
Miller, G. E., & Scalo, J. M. 1979, ApJS, 41, 513
Murray, A. C. 1983, Vectorial Astrometry (Bristol: Hilger)
Nidever, D. L., Marcy, G. W., Butler, R. P., Fischer, D. A., & Vogt, S. S. 2002, ApJS, 141, 503
Reid, I. N., & Cruz, K. L. 2002, AJ, 123, 2806
Reid, I. N., et al. 2002a, AJ, submitted
Reid, I. N., & Gizis, J. E. 1997, AJ, 113, 2246 (RG97)
Reid, I. N., Hawley, S. L., & Gizis, J. E. 1995, AJ, 110, 1838 (erratum 111, 2469 [1996]) (PMSU1)
Reid, I. N., et al. 1999, ApJ, 521, 613 (R99)
Reid, I. N., Kirkpatrick, J. D., Liebert, J., Gizis, J. E., Dahn, C. C., & Monet, D. G. 2002b, AJ, 124, 519
Salim, S., & Gould, A. 2002, ApJ, submitted (astro-ph/0206318)
Salpeter, E. E. 1955, ApJ, 121, 161
Schaller, G., Schaerer, D., Meynet, G., & Maeder, A. 1992, A&AS, 96, 269
Schmidt, M. 1968, ApJ, 151, 393
Ségransan, D., Delfosse, X., Forveille, T., Beuzit, J.-L., Udry, S., Perrier, C., & Mayor, M. 2000, A&A, 364, 665
Siegel, M. H., Majewski, S. R., Thompson, I. B., & Reid, I. N. 2002, ApJ, 578, 151
Upgren, A. R., Grossenbacher, R., Penhallow, W. S., MacConnell, D. J., & Frye, R. L. 1972, AJ, 77, 486
Vyssotsky, A. N. 1956, AJ, 61, 201
Weis, E. W. 1986, AJ, 91, 626
———. 1987, AJ, 93, 451
———. 1988, AJ, 96, 1710
———. 1996, AJ, 112, 2300
Wielen, R. 1974, Highlights Astron., 3, 395
———. 1977, A&A, 60, 263
Wielen, R., Jahreiss, H., & Krüger, R. 1983, in IAU Colloq. 76, The Nearby Stars and the Stellar Luminosity Function, ed. A. G. D. Philip & A. R. Upgren (Schenectady: L. Davis), 163
Wilson, R. E. 1953, General Catalogue of Stellar Radial Velocities (Carnegie Inst. Washington Publ. 601) (Washington: Carnegie Inst.)